UNIVERSIDADE FEDERAL DE SÃO CARLOS
CENTRO DE CIÊNCIAS EXATAS E DE TECNOLOGIA
DEPARTAMENTO DE QUÍMICA
PROGRAMA DE PÓS-GRADUAÇÃO EM QUÍMICA

“Synthesis, Characterization and Cytotoxicity of Pd(II) Complexes for the Inhibition of Cathepsin B.”

Amos Olalekan Akinyemi*

Dissertation presented as part of the requirement to obtain the title of MASTER’S IN CHEMISTRY, concentration area: INORGANIC CHEMISTRY.

Advisor: Prof. Dr. Fillipe Vieira Rocha

***Scholarship Holder: CAPES**

SÃO CARLOS – SP

2021

UNIVERSIDADE FEDERAL DE SÃO CARLOS

Centro de Ciências Exatas e de Tecnologia
Programa de Pós-Graduação em Química

Folha de Aprovação

Defesa de Dissertação de Mestrado do candidato Amos Olalekan Akinyemi, realizada em 13/12/2021.

Comissão Julgadora:

Prof. Dr. Fillipe Vieira Rocha (UFSCar)

Prof. Dr. José Clayston Melo Pereira (UNESP)

Profa. Dra. Roberta Cerasi Urban (UFSCar)

O presente trabalho foi realizado com apoio da Coordenação de Aperfeiçoamento de Pessoal de Nível Superior - Brasil (CAPES) - Código de Financiamento 001.
O Relatório de Defesa assinado pelos membros da Comissão Julgadora encontra-se arquivado junto ao Programa de Pós-Graduação em Química.

Even though learning has no end, praises
be to GOD for his inexpressible gift.

DEDICATION.

I dedicate this thesis to my family for nursing me with affections, love, and their dedicated partnership for success in my life.

ACKNOWLEDGEMENT.

First and foremost, I thank God for everything that exists and for studying science and getting to know you better through it.

I want to express my sincere thanks to my practical, judicious, and efficient **Prof. Dr. Fillipe Vieira Rocha** for all the support and attention and for being willing to work as a team. May your continuity be like a golden fish that has no hidden place. I am honored to be one of your students. Hence, having a supervisor like you is such an inspiration for me to keep going. As Chadwick Boseman once said, “you have to cherish things in a different way when the clock is ticking.” I cherish the two years plus I spent with you differently, my dear Professor. Thank you once more for the opportunity to conduct this research in your laboratory—the research powerhouse.

Another cogent factor that influenced the success of this work is a conducive work environment. I thank my laboratory colleagues: Mauro (Micky), Vito (Vitao), Lucas, Debrah (Waze), George (Cenoura Pequena), Josias (homem do Café), Vinicus (Costa), Dairo and Gabriela (Gabi). I appreciate everyone for the warm welcome given to me as an international student in the laboratory. Even though the pandemic almost hampered the visibility way of interaction, I appreciate the friendship, company, and jocular way of interacting gathered in this time. I have gained a deeper understanding of how many advances in society are made through cooperation rather than a ruthless competition. The very fabric of humanity is a collaborative effort.

I owe a special thanks to Mauro Almeida Lima for his unwavering support through the creation of this work. Notwithstanding the minor language barrier, you made things work whenever I beckon on you. I will boldly say that I kowtow.

Moreover, I sincerely appreciate all professors (Prof. Jean Gallo, Prof. Augustin Hernanadez, Prof. Catherina Cunha, Prof. Julio Zukerman, and others) in the department of chemistry who added values and academic cultures in me during the classes I took. Most importantly, I appreciate the Federal University of São Carlos and the department of chemistry (DQ) for providing the structure, equipment needed for

conducting this research. And to technicians and all professionals committed to teaching and developing science.

To the funding agencies FAPESP, CNPq, and above all, to the Coordination for the Improvement of Higher Education Personnel (CAPES) for funding this work. Because without it, this work would not have been done.

Finally, I will progress by saying, between the beginning and the end, there is always a middle. The middle thanks go to those – Dr. Bolaji Charles, Amanda Santos Pereira, Dr. Elijah Anertey, Olamide Olaoba, Kehinde Ayinde, John Teibo, Prof. Marcelo, Iara Araujo, Jennifer Oluwakemi Odedeyi, Charles Olaosebikan Omisore, Zaccheaus Alabi– who made my leisure time fun-filled.

I thank the Coordination for the Improvement of Level Personnel Superior – Brazil (CAPES)- Financing Code 001.

List of Abbreviations.

AD	Alzheimer's disease
CTC	Circulating tumor cells
CTSB	Cathepsin B
DMF	Dimethylformamide
DMSO	Dimethyl sulfoxide
DNA	Deoxyribose Nucleic acid
ECM	Extracellular matrix
ESI-MS	Electron spray ionization mass spectrometry.
LMCT	Ligand-to-metal charge-transfer
M6P	Mannose-6-phosphate
MDR1	Multidrug resistance protein inhibition
MLCT	Metal-to-ligand charge-transfer
MMPs	Matrix metalloproteinases
NMR	Nuclear Magnetic Resonance
pH	hydrogenic potential
ROS	Reactive Oxygen Species
RR	Ribonucleotide reductase
TIMP-1&2	Tissue inhibitor of metalloproteinases 1 and 2
TSCs	Thiosemicarbazones
uPA	Urokinase protease activity
VEGF	Vascular endothelial growth factor
SCN	Thiocyanate
TSC	Thiosemicarbazone
UV-vis	Ultraviolet-visible region

List of Tables.

List of Figures.

x

Molecular Structures and Masses of Compounds.

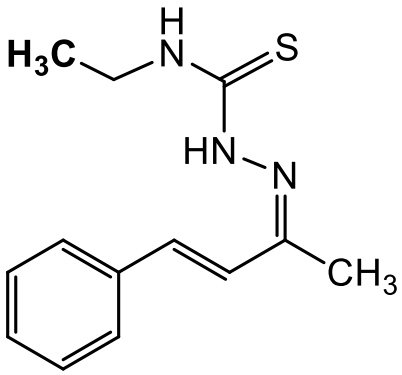

TSC

Molecular Mass 91.13g/mol

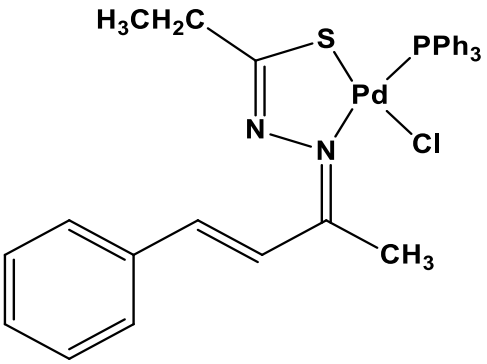

[Pd(TSC)ClPPh$_3$] (1)

Molecular Mass 651.51g/mol

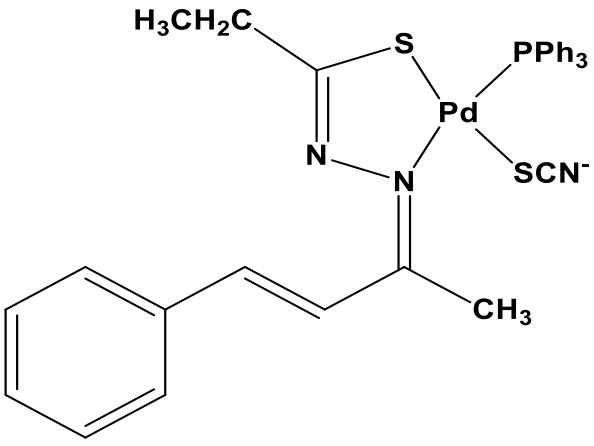

[Pd(TSC)SCNPPh$_3$] (2)

Molecular Mass 674.15g/mol

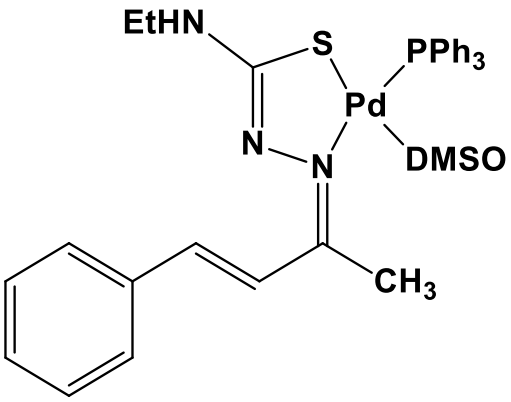

[Pd(TSC)(DMSO)PPh$_3$] (3)

Molecular Mass 649.20g/mol

Resumo.

Síntese, caracterização e citotoxicidade de complexos de Pd (II) para a inibição da catepsina B.

O câncer é uma das doenças mais temidas do século XX, e sua prevalência e incidência estão aumentando no século XXI. A situação é tão grave que uma em cada quatro pessoas pode desenvolver câncer durante a vida. Existem vários componentes que influenciam o crescimento do tumor, indicando múltiplas vias para o desenvolvimento de novos compostos quimioterápicos com diferentes modos de ação. A enzima catepsina B, por exemplo, está relacionada a formação de novos vasos sanguíneos que nutrirão o tumor e a progressão tumoral. Esta enzima é superexpressa em vários tipos de câncer, incluindo câncer de próstata, pulmão e mama. Nesse sentido, a busca por compostos capazes te inibirem a ação desta enzima é extremamente desejável. Os complexos de Paládio (II) podem ser uma alternativa promissora para a obtenção de moléculas com forte citotoxicidade e capacidade de bloquear a atividade da Catepsina B, uma vez que podem se ligar de forma efetiva ao sítio ativo da enzima alvo. Para tal, incorpora-se ao arcabouço molecular um ligante tiossemicarbazona e a trifenilfosfina, gerando compostos do tipo [Pd(TSC)XPPh_3] [(X = Cl^-; SCN^-; DMSO), PPh_3 = Trifenilfosfina, TSC = 1- metil-3-fenilprop-2-en-1-ilideno hidrazina carbotioamida). Após a completa caracterização dos complexos por diferentes técnicas, ensaios de citotoxicidade foram realizados frente a três linhagens celulares [PNT2 (células não tumorais da próstata), A2780 Cis (linhagens tumorais de ovário) e MRC5 (células pulmonares não tumorais)], os resultados indicam uma elevada citotoxicidade dos complexos, superando o valor do fármaco padrão cisplatina em até 1400 vezes, no entanto, não foi perceptível uma preferência entre células tumorais e não tumorais. Além disso, ensaios de titulação espectrofotométrica com o DNA foram realizados para investigar se existe alguma interação entre eles. Os resultados mostraram uma fraca ou nenhuma interação entre eles, portanto, o DNA foi descartado como um possível alvo citotóxico. No entanto, a partir dos dados de ensaio de inibição das enzimas topoisomerases, foi possível observar a capacidade de impedir o relaxamento do DNA causado pela enzima topoisomerase I beta, indicando que este pode ser um dos alvos farmacológicos destes complexos. Adicionalmente, os compostos mostraram serem

capazes de inibir de forma irreversível a ação da catepsina B em concentrações menores que 100 uM. Diante disso, conclui-se que este tipo de composto pode apresentar características estruturais interessantes para fornecer compostos metálicos que inibem a progressão do câncer.

Abstract.

Synthesis, Characterization and Cytotoxicity of Pd(II) Complexes for the Inhibition of Cathepsin B

Cancer is one of the most dreaded diseases of the 20th century, and its prevalence and incidence are increasing in the 21st century. The situation is so serious that one in four people can develop cancer in their lifetime. Several components influence tumor growth, indicating multiple pathways for developing new chemotherapeutic compounds with different modes of action. The enzyme cathepsin B, for example, is related to the formation of new blood vessels that will support the tumor and tumor progression. This enzyme is overexpressed in many types of cancer, including prostate, lung, and breast cancer. In this sense, the search for compounds capable of inhibiting the action of this enzyme is extremely desirable. Palladium (II) complexes may be a promising alternative for obtaining molecules with strong cytotoxicity and the capacity to block the activity of Cathepsin B. Once they can effectively bind to the active site of the target enzyme. Hence, a thiosemicarbazone ligand and triphenylphosphine are incorporated into the molecular framework, generating compounds of the type [Pd(TSC)XPPh3] [(X = Cl-; SCN-; DMSO), PPh3 = Triphenylphosphine, TSC = 1-methyl- 3-phenylprop-2-en-1-ylidene hydrazine carbothioamide). After complete characterization of the complexes by different techniques, cytotoxicity assays were performed against three cell lines [PNT2 (non-tumor prostate cells), A2780 Cis (ovarian tumor lines), and MRC5 (non-tumor lung cells)]. The results indicate high cytotoxicity of all complexes, surpassing the value of the standard drug cisplatin by up to 1400 times. However, a preference between tumor and non-tumor cells was not noticeable.

Furthermore, spectrophotometric DNA titration assays were carried out to investigate any interaction between them. The results showed weak or no interaction. Therefore, DNA was ruled out as a possible cytotoxic target. Nevertheless, from the topoisomerase inhibition assay, it was possible to observe the ability to prevent DNA relaxation caused by the topoisomerase I beta enzyme, indicating that this may be one of the pharmacological targets of these complexes. Additionally, the compounds were

shown to irreversibly inhibit the action of cathepsin B at concentrations lower than 100 uM. Therefore, it is concluded that this type of compound can present interesting structural characteristics to provide metallic compounds that inhibit cancer progression.

Table of Contents

1.0 Introduction

1.1 Cathepsin

Cathepsins are largely expressed lysosomal proteases that source from papain family found in all mammalian cells [1, 2]. The name “cathepsin” was inferred from the ancient Greek word “Katahepsin” which implies “to digest” [1]. More than dozen cathepsins have been identified in various organisms, examples include Cathepsin A, B, C, D, E, F, G, H, J, K, L, O, S, T, V, W, Y, Z [3-19]. Hence, out of those mentioned above, there are 11 members in the human cysteine cathepsin family (Cathepsin B, C, H, F, K, L, O, S, V, W, X/Z) and 19 members in mouse [8, 20]. In a normal cell, cysteine cathepsins have roles in antigen presentations, apoptosis, autophagy and cellular homeostasis [21-23]. In cancer, the cellular localization of lysosomal cysteine cathepsins is often altered. intracellular, cell surface, and secreted cysteine cathepsins are involved in distinct tumorigenic processes in vivo, such as angiogenesis, invasion through extracellular matrices, and metastasis [24, 25].

1.1.1 Cathepsin B

Cathepsin B is the most intriguing, due to its core role in health and diseases [26]. It is a cysteine protease that performs a significant role in metalloproteinases regulation and it is structurally comparative to the papaya enzyme papai [27]. Cathepsin B has been found to be located on chromosome 8p22. The CTSB gene, also known as the cathepsin B gene, is made up of 13 exons [28, 29] (Figure 1.1). Studies have shown that cathepsin B is significant as it is involved in various pathologies and oncogenic processes [30]. In a typical physiological condition, cathepsin B is firmly directed at series of levels in a well-coordinated manner. However, the regulation of cathepsin B can be altered in multiple levels during malignant transformation resulting in overproduction [31]. Cathepsin B overexpression has been observed in a variety of cancers, including breast, colorectal, and lung cancer and other variety of human disease like rheumatoid arthritis, osteoarthritis, Alzheimer’s diseases (AD), and pancreatitis [32, 33]. Cathepsin B is an important autophagy molecule, playing a significant role in maintaining the physiological function under normal conditions [34]. It has also

been implicated that cells acquire an oncogenic character due to the abnormal regulation of cathepsin B [35].

Kuang and his colleagues recently demonstrated that the translocation of the lysosomal cysteine protease cathepsin B (CTSB) into the nucleus is a key molecular event that promotes organelle-specific activation of ferroptosis in human pancreatic cancer cells [36].

FIGURE 1.1-Conformation of Cathepsin B [37].

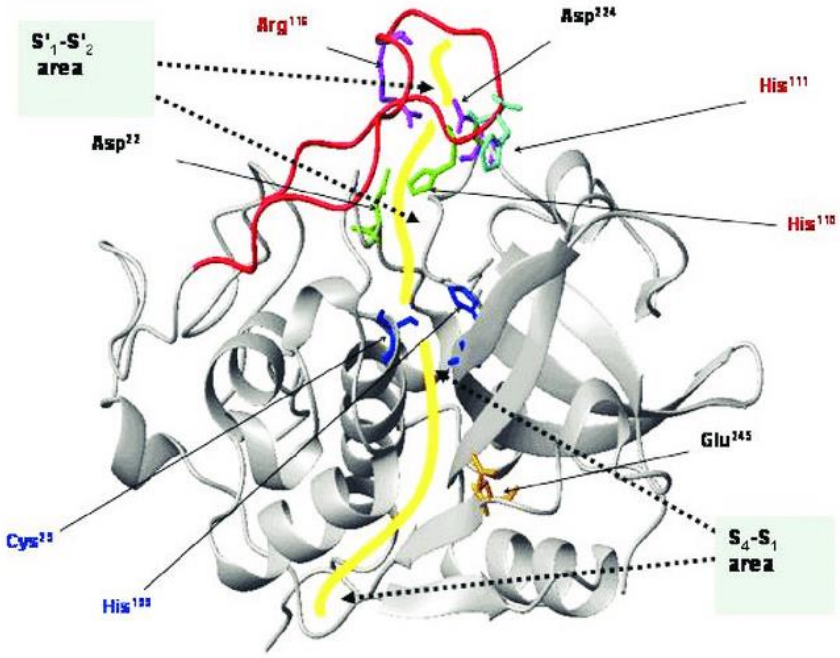

1.1.2 Overall structure of Cathepsin B

Most of the studies performed in 1990 were mostly focused on cathepsin B, which the crystal structure determined [38]. The structure of the enzyme revealed that part of the S2 pocket is formed by the GLU245, a unique residue found only in cathepsin B but not in other cathepsins [38]. Cathepsin B is roughly disc shaped. It is a bilobate protein composed of left and right domains sandwiched by the triad of histidine, cysteine and aspartate residues creating the enzyme catalytic site [38, 39]. The development of cathepsin B composes of light

chain (5kDa) and heavy chain (25-26kDa) linked together by disulfide bond [2]. Cathepsin B differs from other cathepsins with special enzyme characteristics. It has both endopeptidase and exopeptidase activity (carboxyl peptidase) due to the presence of 20 amino acids (Ile105- Thr125) insertion termed occluding loop [40]. Computer aided refinement of cathepsin B crystals structure revealed three contact regions including, prosegment binding loop, occluding loop crevice and substrate binding cleft [41]. Chain forms of cathepsin B is dependent on species and tissue of origin, that is, mature cathepsin B can exist as a single chain shape, double chain shape or as both single and double-chain shape [42, 43].

FIGURE 1.2-Cathepsin B structure that shows the existence of occluding Loop and active sites, making it unique to another Cysteine [43].

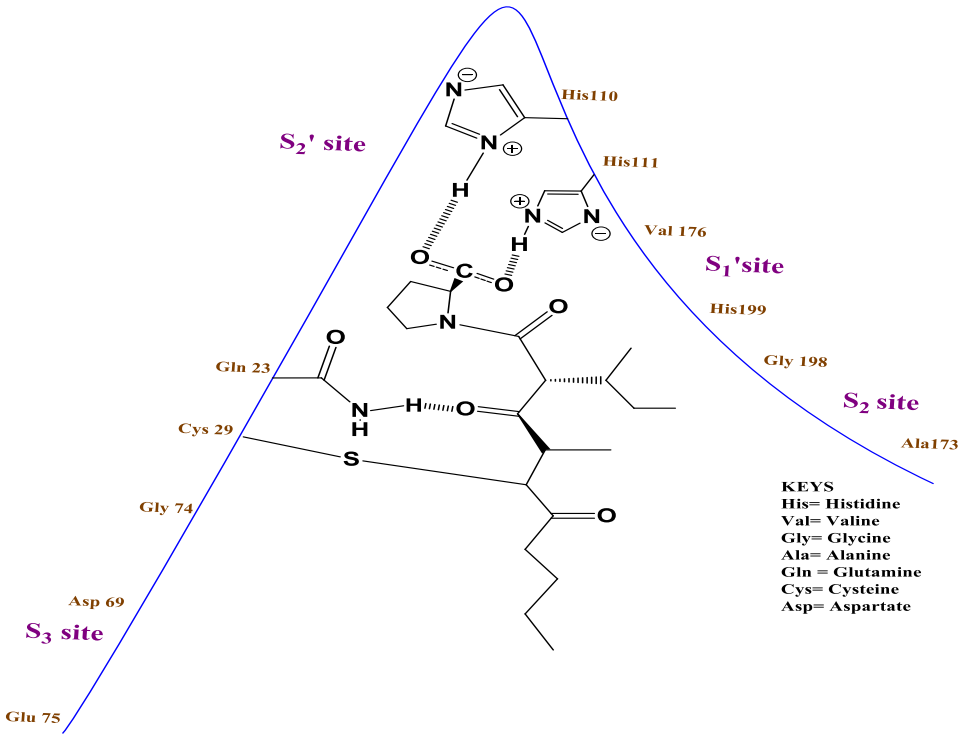

1.1.3 Synthesis and Localization of Cathepsin B

Cathepsin B is initially synthesized as an inert zymogen; a proenzyme that is subsequently converted into its active form when exposed to acidic environment in lysosomes [44-46]. Elaborating on the stages involved, cathepsin

B is synthesized on rough endoplasmic reticulum as preprocathepsin B with a signal peptide of seventeen amino acids. The signal peptide is a molecular address label that targets the proenzyme into the lumen of rough endoplasmic reticulum where the signal peptide is further excluded to form an inert precursor known as procathepsin B. This inert molecule is further transported via the rough endoplasmic reticulum into the golgi apparatus for post-translational modification, including glycosylation at its two asparaginyl residues by phosphorylated moiety of mannose-containing oligosaccharide. The phosphorylated protein further bonded firmly to mannose-6-phosphate (M6P) receptor within the trans-golgi network and it is mobilized via transport vesicles to the lysosomes giving rise to cathepsin B [47] (FIGURE 1.3).

FIGURE 1.3-Preprocathepsin B is synthesized on the rough endoplasmic reticulum where a signal peptide is jointly extracted. The enzyme is glycosylated after transport into the Golgi apparatus. The Mannose-6-phosphate signal is assembled, and mannose 6-phosphate receptors located in the trans-Golgi network are recognized. Procathepsin B is moved to an acidic compartment of receptors in which the enzyme is activated by removing propeptide, which leads to cathepsin B [43].

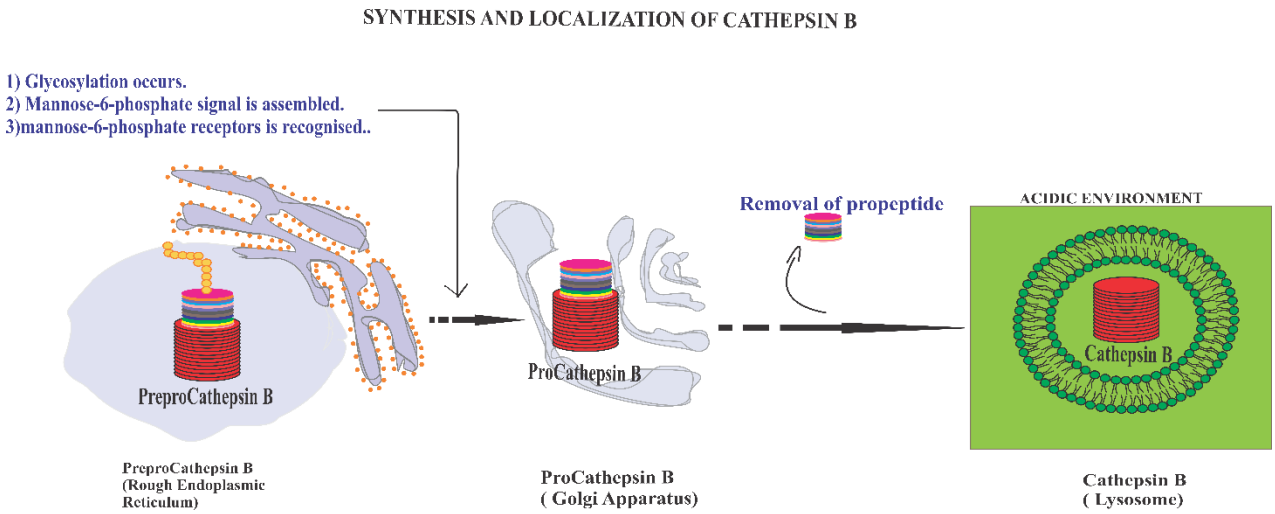

Cysteine cathepsin is located in the digestive vesicle lysosomes where it is mindful for driving proteolytic degradation inside the lysosome [48]. Since lysosomes contain mixed concoction of hydrolytic enzymes, therefore, they can degrade nucleic acid and other biological molecules; take part in the debasement of particles taken up from the extracellular matrix as well as a typical turnover of cellular components [42]. Moreover, under normal physiological condition, cathepsin B is regulated at several levels (such as transcription, post-transcriptional, translation, post-translational processing, and trafficking) and plays different parts within the upkeep of cellular metabolism [49]. In addition, it is expressed in the kidney and other tissue critical to development and breakdown of cellular proteins [50]. In previous time, studies have demonstrated that, active cathepsin B are found in other compartments of the cell like the nucleus (where nuclear scaffold is found to be related), plasma membrane and the cytoplasm, where they contribute to protein turnover and polypeptide degradation [51, 52]. More recently, Padamsey and his colleagues showed that cathepsin B localized in the lysosome controls the long-term dendritic spine structural plasticity, by activating metalloproteinase 9 and remodeling the extracellular matrix [53].Interestingly, aside from the fact that cathepsin B is associated with lysosomes where it is linked to protein degradation, the localization of the cysteine cathepsin in cancer cell changes from lysosomes to vesicles in the peripheral cytoplasm and to the plasma membrane [49]. Wassélius and his colleagues [54] identified cathepsin B to be present in various types of tissues and cell types – such as stromal cells, epithelium, anterior sub capsular lens epithelium, endothelium of the cornea epithelium lining the ciliary processes, at all locations in cytoplasmic granules, and various cell types in the retina – throughout the rat eye.

1.1.4 Increased Expression of Cathepsin B in tumors.

Cathepsin B is highly expressed in human malignancies. A wide range of malignancies have been found to exhibit high amounts of cathepsin B protein and activity. In mice models of breast cancer, overexpression of cathepsin B increased tumor cell invasion; the findings in Bengsch and colleagues studies suggested that cathepsin B increases proteolytic extracellular matrix degradation

which lead to increase invasion [55]. In another view, oncogenes has been shown contribute to increased cathepsin B levels as CHa-ras transformation of breast epithelial cells results in increased cathepsin B expression [56]. Moreover, Cathepsin B is overexpressed in esophageal squamous cell carcinoma tissue, both malignant and pre-malignant, as well as human gastric adenocarcinoma [57]. Additionally, Boa and others were able to show how cathepsin B was overexpressed in endometrial tumor tissue compared to normal tissue, and knocking it out stopped cell growth and malignancy [58]. The cathepsin B gene in tumors consist of 12 or 13 exons, including an exon 2a/b spliced between exon 2 and 3 (FIGURE 1.4) [59]. Increases in cathepsin B expression may also reflect post-translational modifications. The K-ras4Bval12 oncogene transfects colon epithelial cells, resulting in increased amount of cathepsin B protein [60].

FIGURE 1.4- Human cathepsin B exon/intron structure. The solid boxes represent translated sequence, and the empty boxes represent untranslated sequence. Exon were mapped by southern blot hybridization, sequencing and RNase protection assays. Adapted from Berquin et al. [59]

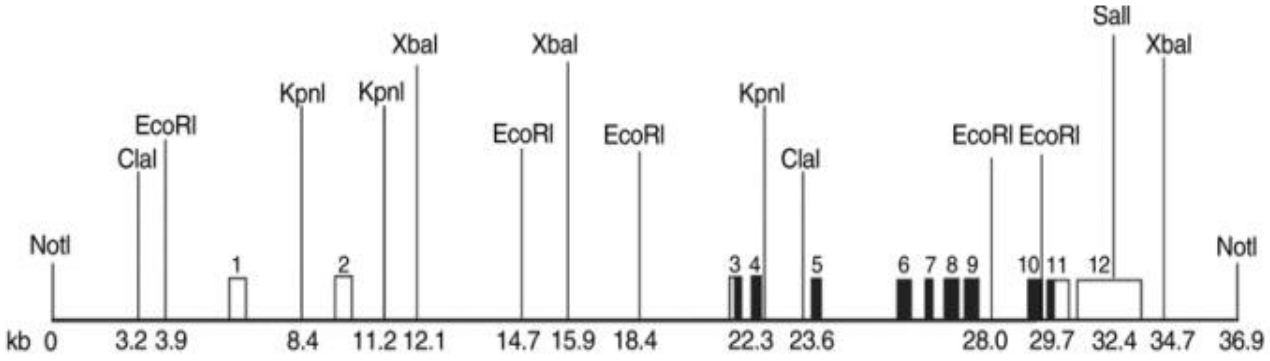

1.2 Cancer

Cancer has advanced as one of the principal causes of death worldwide, it is the cells that grow out of control and invade other tissues. In most basic term, it is one of the diseases causing apex fear in the society due to its

stigma of pain and mortality [61]. However, it is also the third leading cause of death worldwide with 12%, killing about 6.0 billion people a year. Currently, it is the second leading cause of disease deaths in Brazil [61]. Cells may become cancerous due to the defect's accumulation, or mutations, in their DNA. Cancer can spread via the body through blockage by cardiovascular or lymphatic system known as metastasis [62, 63]. Nonetheless, it is a collection of more than 100 diseases characterized by uncontrolled cell growth, which do not have the same function as cells healthy in their original tissues. Due to this high proliferation, which causes the formation of tumors, the cells become very aggressive to the organism and can spreads through different tissues and/or organs of the body, this process is called of metastasis and the main reason for the causes of death (Figure 1.5).

Malignant tumors can extend and invade other tissues. This process is a key characteristic of cancer. Benign tumors grow locally and don't spread. As a result, benign tumor is rarely harmful. They can still be dangerous especially if they press against vital organ like the brain [62]. There are four main types of treatments for 100 tissue types where cancer occurs: bone marrow transplanting, surgical procedure, radiotherapy and chemotherapy [62, 64]. In many cases these treatments are combined. Chemotherapy is a procedure in which medications are administered intravenously, orally, subcutaneously or intramuscularly and is one of the most commonly used cancer treatments [64].

FIGURE 1.5-Diminutive outline showing the process involve in carcinogenesis and formation of tumor, leading to the term cancer [64].

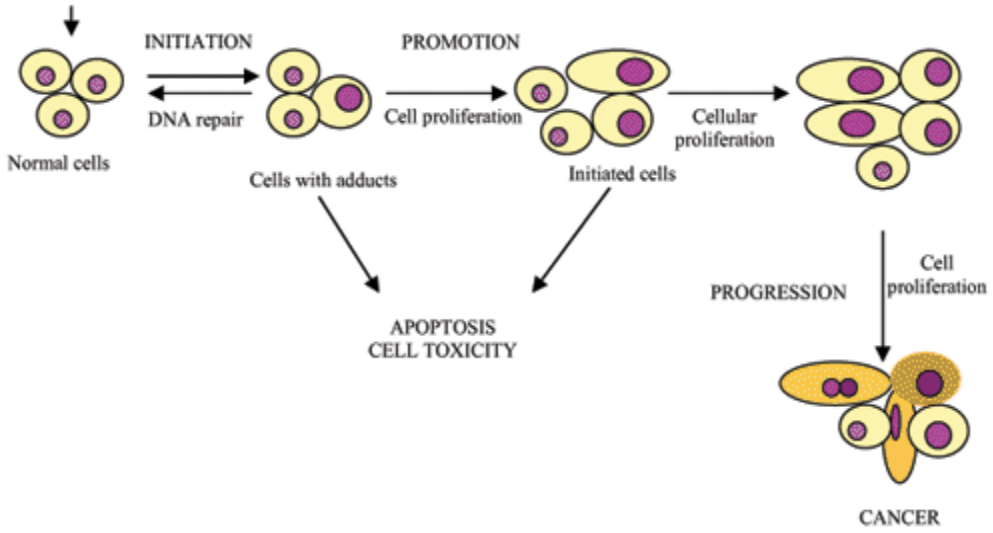

1.3 Role of Cathepsin B in Carcinogenesis.

In normal physiological conditions, cathepsin B is well-coordinated at multiple-levels and important in various oncogenic and pathological processes. However, whenever one of the regulated multiple levels of the cysteine cathepsins is dysregulated, an increase in expression activities and distribution of enzymes within the cells takes place [65]. Cathepsin B overexpression has been implicated in several forms of cancer such as breast cancer [66, 67], lung cancer [68], brain cancer [69], colorectal cancer, and prostate cancer [70, 71].

Cathepsin B is a major player in tumor angiogenesis as well as the metastasis process by hydrolyzing the inhibitors of matrix metalloproteinases (MMPs), tissue inhibitor of metalloproteinases 1 and 2 (TIMP-1 &2), culminating in elevated MMP and further enhancement of extracellular matrix (ECM) degradation, thus allowing the migration of endothelial cells and tumor invasion through the remodeled ECM. [72, 73] (See figure 1). In multicellular organisms, cathepsin B modulates the process of apoptosis, while acting anti-apoptotically or pro-apoptotically [73]. It acts anti-apoptotically via inactivation of Bak (more information from Alabi et al. [74]) and caspase inhibitor XIAP; pro-apoptotically by actuating Bid which triggers the discharge of cytochrome C from the mitochondrial inner compartment into the aqueous compartment of the cytoplasm, where it further actuate caspase 9 [67, 74]. Moreover, this cysteine cathepsin B is efficient in

hydrolyzing the extracellular matrix components such as the laminin, type IV collagen and fibronetic which therefore enable tumor cells to affect the surrounding tissues [75-78]. Cathepsin B has one single copy gene mapping to 8p22 chromosome. However, heightened expression of cathepsin B correlates with concomitant gene amplification which further leads to a novel the 8p22-8p23 amplicon synonymous to cathepsin B gene locus [79-81]. Consequently, the aforementioned was connected to the over-expression of cathepsin B in oesophageal adenocarcinoma [81].

In an attempt to determine cathepsin B as a potential biomarker in cervical cancer, Wu *et al.* [82] observed the expression of cathepsin B in the cell line of cervical cancer (Hela cells). A substantial increase in the expression of cathepsin B was found in invasive carcinomas, in comparison to non-cancerous tissues. Such increase was further paralleled to lymphatic metastasis and tumor invasion depth [82]. In another study, a marked level of cathepsin B resulted to assemble of stromal changes, alongside distinctive mechanisms that get activated beneath the epithelium, culminating in the so-called tumor microenvironment [83]. This, therefore, shows that the pivotal role of cathepsin B in cancer advancement may be via the establishment of an enabling tumor microenvironment. Although the role of cathepsin B has also been reputed in the progression of leukemia [84], its overall mechanism has only been speculated in some cases. However, emergent studies have revealed the exact action of cathepsin B in carcinogenesis. There is an indication that cathepsin B aid tumor migration and exacerbate invasiveness [85]. Western blotting probe, immune histochemistry assay, and SDS-PAGE profiling similarly demonstrate that cathepsin B bestow to the mechanism and operation of invasion of ovarian cancer [86]. Additionally, since cathepsin B has been shown to be over-expressive in many cancers such as colon cancer [87], such sustained upregulation was shown to contribute to nodal metastasis in inflammatory breast cancer patients. It was further hypothesized how the overexpression of caveolin-1 (a protein encoded by CAV1 gene) in inflammatory breast cancer elevates cathepsin B trafficking to the cell surface where it aids inflammatory breast cancer attack on lymphatic vessels and metastasis to lymph nodes [88]. Upregulation of cathepsin B has been linked to the

promotion of angiogenesis through the induction of metalloproteinase-9 and vascular endothelial growth factor [89, 90].

Recently, the role of cathepsin B overexpression in human hepatocellular carcinoma has been uncovered. This cysteine protein has an oncogenic role in hepatocarcinogenesis which further facilitate the migration of cancer cell and invasion. Cathepsin B stimulates Matrix metallopeptidase-9 (92kDa enzyme participating in the hydrolysis of the extracellular matrix also known as type IV collagenase) in human hepatocellular carcinoma [91]. In comparison, cathepsin B's intracellular and extracellular functions have been demonstrated. A study reveals that the activity of intracellular cathepsin B regulates the premalignant cycle and tumor development, whereas extracellular cathepsin B guides invasive colorectal cancer properties. This suggests that cathepsin B is an important player in colorectal tumor growth, metastasis, and invasion [92]. Even though, cathepsin B display a notable feature in interceding apoptosis in myeloma [93], its activities were also measured in human thyroid tissue and have been shown to be vital in the advancement of lymph node metastasis and extra-capsular invasion in human thyroid tumors [94]. Finally, its role in aging has also been revealed [95].

FIGURE 1.6-Depicts the overall contribution of Cathepsin B in cancer which is underscored by its angiogenic and metastatic tropic mechanism.

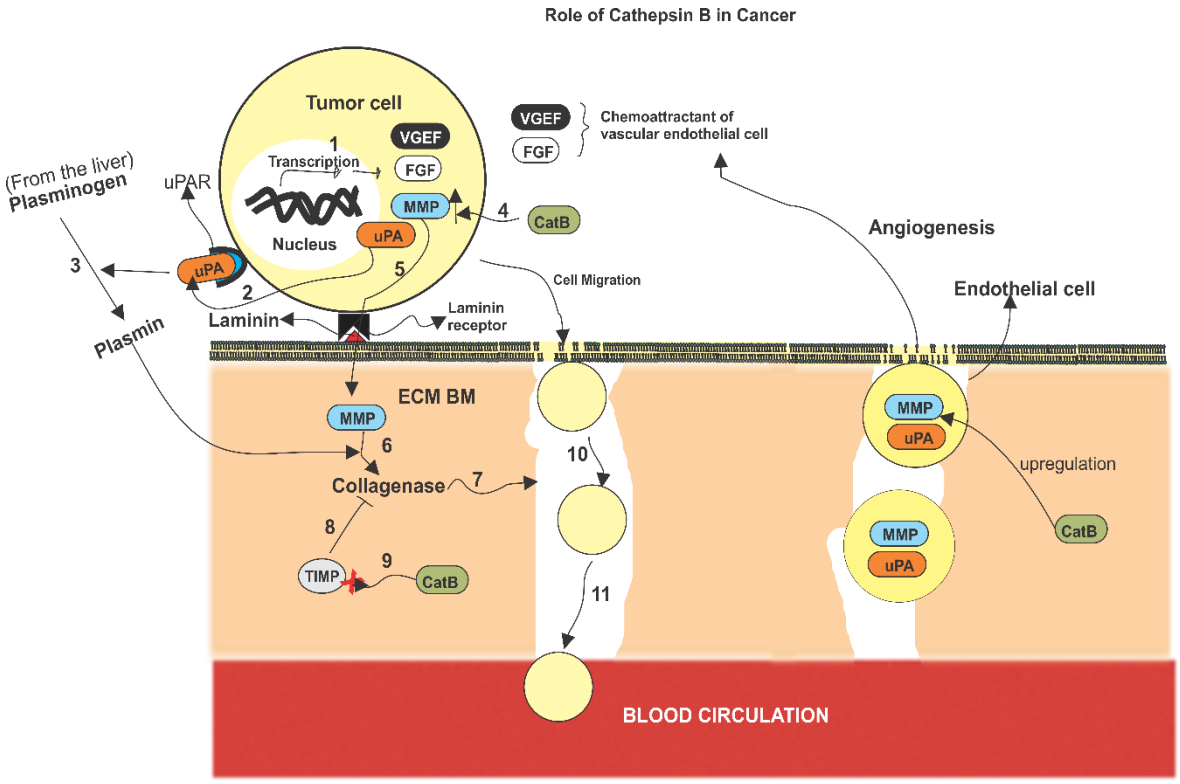

In a primary tumor cell, the upregulation of cathepsin B leads to an increase in transcriptional activity (step 1, 4) culminating in the upregulation of mammalian metalloproteinase (MMP), vascular endothelial growth factor (VEGF), and urokinase plasminogen activator (uPA). The production of uPA both within the cell or the surrounding cell leads touPAR (urokinase plasminogen activator receptor) docking (step 2). The docking, therefore, confers a urokinase plasminogen activator activity on the plasma membrane of the tumor cell. Upon the conferment of uPA activity, the plasma cell, proteolytically activates plasminogen, a zymogen produced in the liver (step 3) and converting it to plasmin. Plasmin directly moves to the basement membrane where it activates MMP (steps 5 and 6). Upon activation, collagenase IV degrades type IV collagen and degrade ECM component such as fibronectin (Step 7). However, another contribution of cathepsin B to tumor metastasis is noticed in the optimization of collagenase activity by complete degradation of the inhibitor of collagenase, TIMP (steps 8 and 9). Once the inhibitor of collagenase is degraded, there is optimization in the activity of collagenase adding to the overall degradation of ECM and BM component leading to the creation of a path, for tumor cell extravasation (steps 10 and 11).

When a tumor cell enters the blood, they become circulating tumor cells (CTC), which can migrate via the blood to a distant organ. Like wisely, we showed here that the angiogenic strategy of cathepsin B is demonstrated through the upregulation of VEGF and FGF, therefore serving as a chemoattractant molecule for vascular endothelial cells, which also expresses mammalian metalloproteinase (MMP). Moreover, cathepsin B upregulates mammalian metalloproteinase in a similar manner to its upregulation. The overall process is similar to the mechanism of metastasis.

1.4 Thiosemicarbazones

Thiosemicarbazones (TSCs) are compounds that possess antitumor, antibacterial, antifungal and antiviral properties [96]. They are compounds that have been studied in the years back for their biological properties. Hence, their actions have been shown to involve interaction with metal ions [97]. One of the most excellent properties for thiosemicarbazone compound is in cancer treatment. Nonetheless, the presence of a metal ion almost systematically increases the activity of the organic parent compounds or helps to attenuate their adverse effects [98]. Currently, the main known effects associated with their anticancer activity are, in order of discovery, Cathepsin B inhibition [99], topoisomerase II inhibition [100], ribonucleotide reductase (RR) inhibition [101], reactive oxygen species (ROS) production [102], mitochondria disruption [103], and Multidrug resistance protein inhibition (MDR1) [104].

Thiosemicarbazones (TSC) have a wide range of applications due to their structural diversity, which allows for the realization of a wide range of substitutions, which can result in different biological responses. They are typically obtained through condensation reactions between thiosemicarbazides and ketones and/or aldehydes and are characterized by simple synthesis with high yields and a wide range of structural possibilities. Another widely held point is that thiosemicarbazones act as strong metal ion sequestering agents, depriving cells of essential metal ions (which can be seen in FIGURE 1.7) [105, 106].

FIGURE 1.7-The diagram below represents the chemical structure and numbering of thiosemicarbazones.

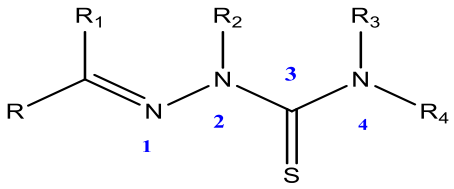

R_1, R_2,R_3 & R_4 =H, akyl or aryl or any organic substituent.

In the work by Reghav and Ravinder, [99] they demonstrated how thiosemicarbazones with a chloro-substituted compounds inhibit cathepsin B most effectively with the Ki value of 1.16 X 10^{-4} and 1.48 X 10^{-5} M respectively. However much, their in vitro studies were further supported by docking results where active site group Cys-29 and His-199 have been found to interact with the compounds under consideration [99]. In Ruiz and his colleagues work [107], they were able to carry out an analysis and inform the scientific world on how thiosemicarbazone with other metal complex exhibit its role in inhibiting cathepsin B. In this their research, they showed how novel phenylthiosemicarbazide (FIGURE 1.8) is a good cathepsin B inhibitor (an enzyme implicated in a number of cancer related events), being the enzyme reactivated by cysteine.

FIGURE 1.8-The diagram below represents phenylthiosemicarbazone that has been implicated to prevent uncontrolled function of cathepsin b. The structure was adapted from Ruiz and his colleagues work [107].

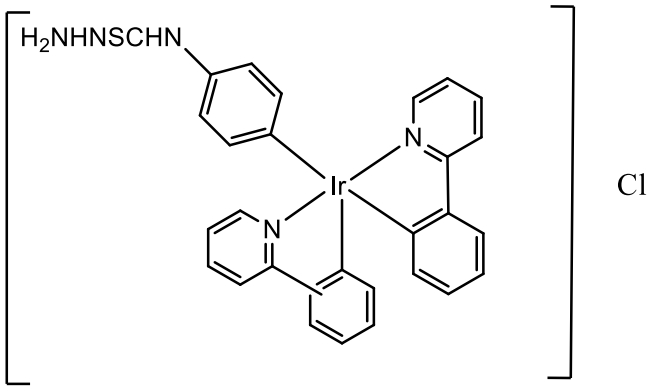

1.5 Metal Complexes

The study of metal complexes in the development of anti-neoplastic developed markedly, especially after the 1970's when cisplatin was approved for clinical use as antineoplastic [108]. Since then, much as been studied about the influence if the center metallic in the biological environment and how the structure of the complex relates to the antineoplastic activity. However much, Transition metal complexes are versatile and have different geometries, being able to coordinate with different organic molecules exhibiting different oxidation states. Furthermore, they can form compounds with positive or negative charges [109, 110].

1.5.1 Palladium

In recent years, remarkable advances in organic and inorganic synthesis via transitional metal complexes have occurred. Among the transition metal complex for organic and inorganic synthesis, those of palladium have had a unique position since 1960. For a long time, palladium had been used in organic synthesis only as a catalyst for hydrogenation. After epoch-making, palladium was recognized as a versatile reagent. Since then, many synthetic reactions using palladium have been discovered [111]. Palladium (II) metal complexes are studied as possible antineoplastic agents, the choice of this metal is due to its similarity to platinum, as both form metallic complexes quadratic planes and may have a metallic ion with a d^8 configuration [112].

The stability of Pd(II) complexes is a little less. As a result, palladium-based compounds might be rapidly hydrolyzed before reaching their target, resulting in minimal antitumour action or even inactivity, as well as toxicity. Furthermore, their relative lability and proclivity for forming trans isomers may stimulate cis-trans isomerization, resulting in inactive species, at least initially [113]. The carrier ligands should be bulky and feature highly coordinating donor atoms such as nitrogen, sulfur, or phosphorus, ideally given by a chelating ligand, to

overcome these drawbacks—that is, to lower the reactivity of the Pd(II) ion. Solid-state structure analysis is also useful in this context for detecting strains, the trans effect, and intermolecular interactions that hold the crystal together [114, 115].

Claudia and the co-authors, for example, were able to demonstrate some biological activity of chiral cyclopalladated complexes with bridging bis (disphenylphosphine) ferrocene ligand as cathepsin B inhibitors and antitumoral drugs. They were able to justify their research by implanting tumor cells (Walker-256 mammary carcinoma) on both sides of an albino rat (see FIGURE 1.9 below). After that, their novel compounds were used to treat the left-hand side. They were able to see that the untreated right side showed constant tumor growth (4.0 1.0g), whereas the left-hand side showed retarred growth of 0.3 1.0g after 12 days (FIGURE 1.10). This demonstrates that the new compounds are effective cathepsin B inhibitors [116].

FIGURE 1.9-Pictorial Illustration of the albino rat with an implant of tumoral cells (walker-256 mammary carcinoma).

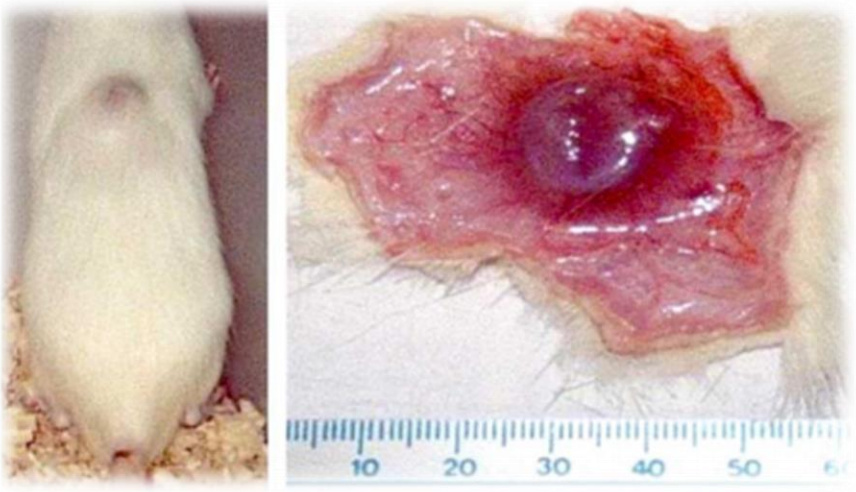

FIGURE 1.10- A rat displaying the variations between the two tumoral cell implants. The rate at which the novel compounds prevent tumoral cells from growing indefinitely on the left hand was shown, but the uncontrolled development on the right hand was shown when no compound was used [116].

1.5.2 The reason for the use of Palladium II complex on Cathepsin B

Palladium (II) complex has high lability and fast hydrolysis reactions in the biological environment. Cathespin B, lysosomal cysteine proteases have a free sulphur atom. The free sulphur atom present in cathepsin B serves as a binding site for palladium (II) complex (i.e Palladium (II) possess great affinity for the cathepsin B sulphur atom). The great affinity occurs because sulphur is a soft base while palladium is a soft acid enabling great relationship concerning the bond and electronic density to take place (Pearson acid-base concept). Generally, the bond with palladium (II) complex and sulphur is extremely strong so this affinity can provide us the likelihood to bring out our complex within the site of the enzyme. The sulphur atom of cysteine present in cathepsin B is involved in formation of the sulfhydryl group which is very reactive. Sulfhdryl group of cysteine can be considered also as a very strong reducing factor, which is very important for activity of many proteins.

FIGURE 1.11-Structural Illustration showing Cathepsin B's sulphur atom, including the site where Palladium II complex will bind.

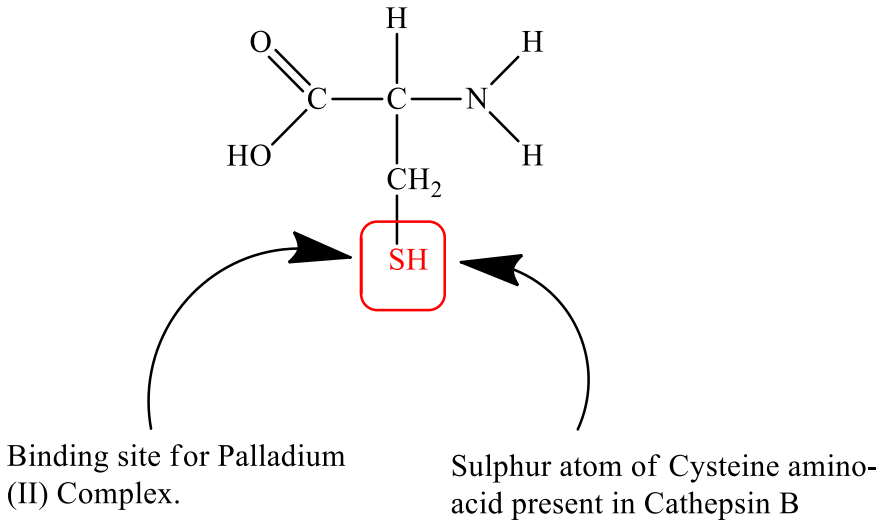

Interestingly, some scholarly articles have been able to use palladium compound to inhibit Cathepsin B via their novel therapeutic approach. For instance, according to Bincoletto *et al.*,[116], they were able to show how [$Pd_2(C_2$, N-$S_{(-)}$ $(dmpa)_2$ (μ-dppf)Cl_2] reversibly supress the operation of cathepsin B activity. It was further elucidated that the novel palladium compound binds cognately to free cathepsin B and to the enzyme-substrate complex. Recently in the year 2019, Askari *et al*.[117] carried out another approach in verifying ability to inhibit cathepsin B. In their research, it was shown that both trinuclear palladium (II) and platinum (II) complexes relatively inhibited cathepsin B in the screening evaluation.

1.6 Structural Planning

Given the facts that the main objectives of this work are to verify the synthesis and characterize Palladium Pd-(II) complexes and also investigate its inhibitory potential and various interactive functions (i.e antineoplastic activities) on cathepsin B. The complex consist fixed ligand: N-Ethyl-2-(1-methyl-3-phenyl-prop-2-ene-1-yl-idene)hydrazinecarbo-thio amide (TSC) and three interchangeable (lability) ligands (Cl^-, SCN, and DMSO). The chosen thiosemicarbazone (TSC) also referred to as fixed ligand is selected because it can react successfully with palladium complex (metal center). Palladium complex is designed with TSC

because TSC provide stability for the complex and also plays vital role in biological activity.

The lability ligands mentioned above are used interchangeably in other to know if there will be a great or lower activity with the sulfur atom. The above stated property will be able to do this when well-coordinated to cathepsin B as a mechanism of inhibiting the biological activities of cathepsin B.

FIGURE 1.12-Planning for the structures of the complexes of the present work.

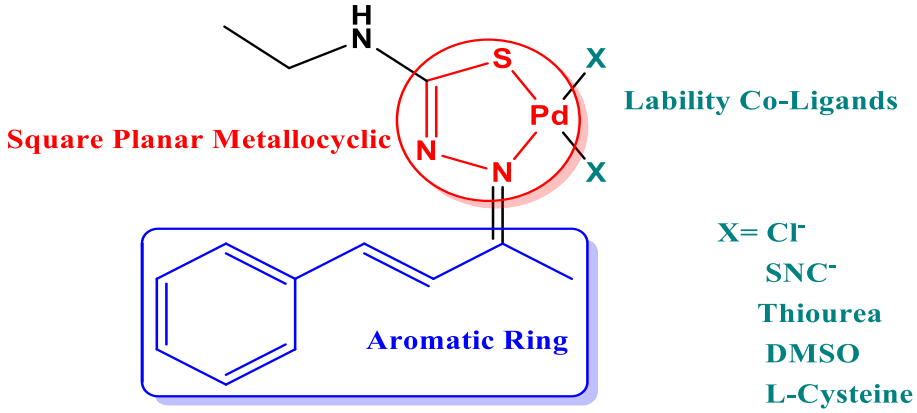

The aromatic ring from the picture shows the location where TSC is located while the square planar metallocyclic is the domain where start complex resides. Considering the lability Co-ligand (X), it elucidates more on how the ligands will be used interchangeably when synthesizing. Obtained complexes will be characterized painstakingly by spectroscopy in the IV, UV-Vis, NMR, mass spectrometry, elementary analysis and X-ray diffraction, if adequate single crystals are obtained, then an evaluation of the cytotoxicity of these compounds will be carried out on cell lines, including both tumor and non-tumor cells. In view of this information, different techniques will be employed to determine the action of the complexes on cathepsin B inhibition.

2.0-Objectives

2.1-Main Objectives:

Obtaining Pd (II) complexes with high cytotoxicity that can inhibit the Cathepsin B action.

2.2- Specific Objectives

- Synthesis of palladium complexes;
- Characterization by different techniques;
- Cytotoxicity assay against non-tumor and tumor of breast, non-tumor and tumor of prostate lines;
- Interaction with DNA via spectroscopic titration;
- Interaction and inhibition with the topoisomerase enzymes;
- Inhibition of the action of cathepsin B.

3-Experimental

3.1 Synthesis

3.1.1 Reagents

In this section, the origin of all the solvents will be described, reagents and methodologies used to acquire results in this work.

TABLE 3.1- Provenance of reagents and solvents.

Reagent	Origin
Dichloromethane	Sigma-Aldrich
Dimethyl sulfoxide (DMSO)	Synth®
Potassium hexafluorophosphate (98%)	Sigma-Aldrich
Palladium (II) Chloride (99%)	Sigma-Aldrich
Potassium thiocyanate	Sigma-Aldrich
Methanol	Synth®
Acetonitrile	Synth®
4-Methyl-3-thiosemicarbazide (97%)	Sigma-Aldrich
Benzalacetone (≥98%)	Sigma-Aldrich
Triphenylphosphine (99%) Sigma-Aldrich	Sigma-Aldrich

3.1.2 Synthesis Methodology

3.1.2.1 Synthesis of Thiosemicarbazone (TSC) [118]

In a 250 mL round, bottom flask was added 0.20 g of 4-methyl-3-thiosemibarzide (1.90 mmol) and 0.28 g of benzalacetone (1.90 mmol) solubilized in 50 ml of ethanol. Then 5 drops of concentrated HCl were added, acting as a catalyst. The condensation reaction was refluxed for 24 h. At the end of the reaction the solution was concentrated in a rota evaporator, cooled in a bath of ice, and filtered. Afterwards, ice-cold ethanol was used to wash the product. Afterwards, the solid was dried under a desiccator. (Obtained 0.23 g of dry mass, 53% yield).

3.1.2.2 Synthesis of the precursor complex $[Pd(CH_3CN)_2Cl_2]$ [119]

In a 125 mL Erlenmeyer flask with 50 mL of acetonitrile previously heated to 80ºC, 500 mg of palladium (II) chloride was slowly added, after the addition of the salt, the formation of a yellow-colored solution was observed. After 4 hours of reaction the solution was concentrated by solvent evaporation and the yellow solid was filtered off. (0.585 g of $[PdCl_2(CH_3CN)_2]$ was obtained, 80% yield).

FIGURE 3.1- Scheme of the synthesis of the complex [Pd $(CH_3CN)_2Cl_2$]

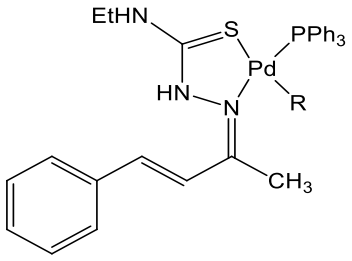

3.1.2.2 Synthesis of $[Pd(TSC)ClPPh_3]$ (1) [100]

The synthesis was adapted from literature. In a 25 mL beaker 15 mL of acetonitrile was added, 50,0 mg (0,19 mmol) of $[PdCl_2(CH_3CN)_2]$ and 47,0 mg (0,19 mmol) of ligand TSC-CC was solubilized in the acetonitrile. After 24h, 51,0 mg (0,19 mmol) of PPh3 was added in the reaction and waited more than 24h. In the end of reaction, the solid form was filtered and dry (Obtained 0.25 g of dry mass, 54% yield).

FIGURE 3.2- Scheme of the synthesis of the complex $[Pd(TSC)ClPPh_3]$\

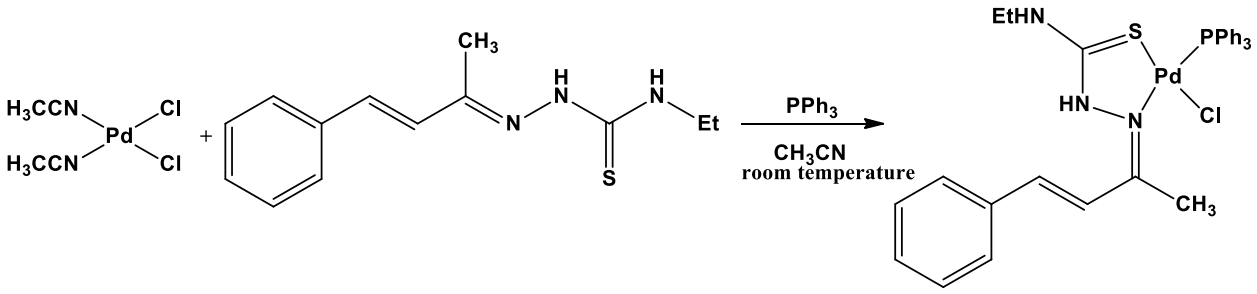

3.1.2.3 Synthesis of [Pd(TSC)SCNPPh$_3$] (2) [120]

In a 25mL beaker, 10mL of methanol was added. However, 50mg (0.077mMol) of my palladium complex [Pd(TSC)ClPPh3] was weighed out and solubilize in the solvent. Addition of 15mg of KSCN follows, which was dissolved in 1mL of water in the reaction as well (Note: colour changes took place from light orange to deep orange colour). The time for the reaction was 20minutes. At the end of the reaction, the solid form was filtered and stored. (Obtained 0.23 g of dry mass, 53% yield).

FIGURE 3.3-Scheme of the synthesis of the compound [Pd(TSC)SCNPPh$_3$]

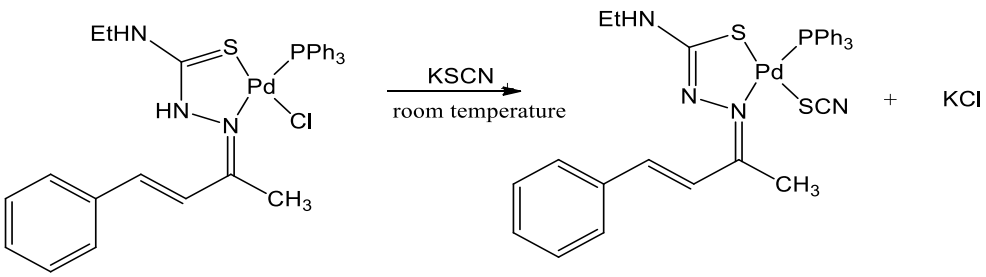

3.1.2.4 Synthesis of [Pd(TSC)(DMSO)PPh$_3$] (3) [121]

At first, 50mg of Palladium complex [Pd(TSC)ClPPh$_3$] was dissolved in 20mL of dichloromethane (CH_2Cl_2). However, further addition of 8.20 micro liter of DMSO took place. The reaction was refluxed and stirred overnight. The solution was allowed to cool down. After cooling down, the synthesis was kept for 3days in the fridge to allow evaporation to take place. However much, 98% of KPF_6 (Potassium hexafluorophosphate) was added and warmed. The precipitate formed was further filtered and weighed. (Obtained 0.31 g of dry mass, 56% yield).

FIGURE 3.4-Scheme of the synthesis of the compound [Pd(TSC)(DMSO)PPh$_3$]

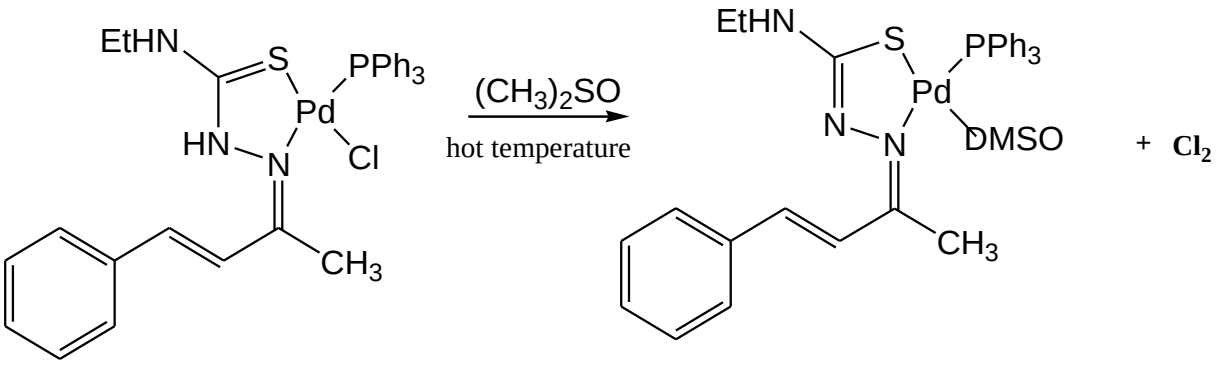

3.2 Instrumental Methods and Procedures

3.2.1 Electronic spectroscopy in the UV-Vis region

The spectra in the visible ultraviolent region were obtained with the help of a SHIMADZU UV-1650PC spectrophotometer. Since, the characterization of the complexes was carried out in chloroform 4.86 X 10^{-5} mol/L, using buckets of quartz with optical path of 1cm ad the scan was made in the region of 200 to 700nm. Hence, the spectra were obtained and processed using UV Prob 2.42 and Origin software 8.0 respectively. During the experiments, baselines were obtained using the acquisition software and the white was subtracted using second beam of light.

3.2.2 Nuclear Magnetic Resonance

To obtain nuclear magnetic resonance spectra of ^{1}H, $^{13}C\{^{1}H\}$ and $^{31}P\{^{1}H\}$ (NMR), THE BRUKER ARX 9.4 Tesla spectrometer from the Department of Chemistry (DQ) at UFSCar was used. The sample were prepared using 2mg of the compounds, which was further dissolved in 500µL $CDCl_3$. All data obtained were treated using the software Mestre Nova 6.0.2-5475. The ^{31}P NMR spectrum was taken just after the ^{1}H resonance, and the measurement was carried out in the same deuterated solution.

3.2.3 Vibrational Spectroscopy in the Infrared region

The absorption spectra in the infrared region were obtained on the SHIMADZU IR Tracer- 100 spectrometer using KBr inserts as support. Hence, 32 scans for greater accuracy were performed in the region from 4000 to 400 cm^{-1}. The data obtained were further processed using Shimadzu IR solution software, 1.60 and Origin 8.0.

3.2.4 Elemental Analysis (CHN)

Elemental Analysis were performed using CE instruments Fission equipment, model CE1108 (CHNS-O) EAGER 200-RESULTS. The person responsible for the analysis was “Luciana Visoto”, a technician from the chemistry department at UFSCar. The method used for analysis was CHNS1904, using a sulfanilamide standard to calibrate the equipment with a mean error of ± 0.05 for percentage of carbon; ± 0.18 for percentage of hydrogen; and ± 0.09 for percentage of nitrogen.

3.2.5 Mass Spectrometry

After diluting the sample at the concentration of 500.0 mg. mL^{-1} was using an ultra high efficiency liquid chromatograph for flow injection and increased collision energy (0, 20 and 40 eV). In this analysis, a phase was used drag mobile consisting of water (solvent A) and acetonitrile (solvent B) with 0.1% formic acid (v/v). The flow was 0.400 mL.min−1 with an injection volume of 10.0 µL. The qualitative analysis of the compounds was performed in the positive mode being used the following parameters for ionization. TABLE 3.2:

TABLE 3.2 - Parameters used for ionization using ESI.

Gas temperature (°C)	250
Gas flow (l/min)	8
Nebulizer (psi)	45

Gas thermal barrier temperature (°C)	300
Temperature of the thermal flow barrier (°C)	11
Nuzze Voltage (V)	0
Shredder (eV)	350
Skimmer	65

Molecular ion and fragment ions were simultaneously obtained by MS2 acquisition mode. Spectra were acquired by monitoring a range between 100 and 1,500 Da and processed by Mass Hunder Workstation version software B.08.00

3.2.6 Single Crystal X-ray diffraction

X-ray diffraction was performed by doctoral student João Honorato (LERCI-UFSCAR) in collaboration with Prof. Dr. Eduardo Ernesto Castellano (IFSC-USP) from the Crystallography Laboratory of the Institute of Chemistry of São Carlos (IQSC-USP), using a Rigaku XtaLAB mini II diffractometer, MoKα radiation (λ = 0.71073 Å). The structure was solved with the SHELXT program using direct methods, successive Fourier-Difference maps allowed the location of non-hydrogen atoms. Except for the hydrogen atoms, all others have been refined anisotropically. The refinements were made using the least squares method using the SHELXL program [122-124].

3.2.7 Cytotoxicity

Cytotoxicity assays were performed using the following cell lines: (PNT2 (Non-Tumor Prostrate cell), A2780 Cis (Ovarian tumor cell lines) and MRC-5 (non-tumor lung cell)). The cells were cultivated in DMEM medium (Dulbecco Modified Eagle Medium) with 10% (v/v) of FBS (fetal bovine serum) inside plastic bottles (Corning) stored in an oven at 37ºC with 5% CO_2 atmosphere. Cell counting

was performed using Trypan Blue dye in a Neubauer chamber on the Nikon Eclipse TS100 Microscope. After counting the suspension, aliquots of 150 µL containing 1.5x104 cells mL-1 were added to 96-well plates. The plates were kept for 24 h in the oven and then 0.75 µL of a DMSO solution containing the ligand or complexes was added to each well. The final concentrations of compounds in the wells were $8.00x10^{-1}$; 1.58; 3.16; 6.25; 12.50; 25.00; 50.00; 100.00 µmol·L^{-1}; for the most active compounds the concentrations needed to be adjusted to: $2.00x10^{-1}$; $3.90x10^{-1}$; $7.80x10^{-1}$; 1.58; 3.16; 6.25; 12.50; 25.00 µmol·L^{-1}. Then, the plates were incubated again in the oven for another 48 h [125-127].

After incubation of the microplates, 50 µL of an MTT solution (3-(4,5-Dimethylthiazol-2-yl)2,5-Diphenyl Tetrazolium Bromide) (1 mg·mL^{-1}) was added to each well and incubated again in the greenhouse for 4h. Finally, the solution was removed from each well and 100 µL of DMSO was added, then absorbance measurements were taken in each well with BioTek's hybrid microplate reader model SYNERGY H1. The data obtained were treated using Excel 2010 and GraphPadPrism 5.01.

3.2.8 Interaction with ct-DNA by visible ultraviolent spectroscopy

To perform the DNA interaction test, first, it was an aqueous solution of 10.0 mmol.L^{-1} of tris-HCl, 10.0 mmol.L^{-1} of NaCl is prepared (pH = 7.4) at room temperature. In this work, a stock solution of Calf thymus/ct-DNA. DNA from calf thymus. (ct-DNA) 1mg/mL was prepared in tris-HCl solution at 4 - 9°C. Before the procedure, the solution was stored in a refrigerator at approximately 4°C to avoid degradation of the biomolecule and the reason of the absorbance wavelengths 260 and 280 nm (A260 / A280) above 1.8 indicating that ct-DNA has the acceptable number of contaminating proteins that can harm the interaction with the compounds studied. To determine the concentration molar DNA in the solution, the molar absorptivity (ε = 6600 L.mol^{-1}) was used .cm^{-1} ; λ = 260 nm) reported in the literature [128]. After obtaining concentration through the Law of Lambert-Beer, equation 3, the solution was diluted to 10^{-3}mol.L^{-1}.

Equation 3: Lambert-Beer Equation, in “A” is the absorbance, “l” the optical path, “ε” the molar absorptivity and “c” the concentration of the chemical species.

$A = \varepsilon . c . 1$

The binding constant (K_b) was calculated using the titration technique spectrophotometric. The binding constant of the complex with ct-DNA was determined by applying the modified Benesi–Hildebrand Equation, as shown in EQUATION 1.0 [114, 116].

$[Complex]/(\varepsilon A - \varepsilon F) = [Complex]/(\varepsilon B - \varepsilon F) + 1/Kb\ (\varepsilon B - \varepsilon F)$

Where: [Complex] = added concentration of the complex.

εA = Abs/[Complex]

εF = free DNA molar absorptivity coefficient and

εB = molar absorptivity coefficient of the DNA-bound complex.

EQUATION 1.0 – Benesi-Hildebrand Equation.

Through the slope and intercept of the linear fit of [Complex] / [εa - εf vs [Complex] we have 1/ [εa - εf] and 1/ Kb [εb - εf]. The intrinsic binding constant Kb can be obtained from the slope-to-intercept relationship.

3.2.9 Inhibition of the DNA- topoisomerase I Beta enzyme

The DNA-Topoisomerase I β enzyme inhibition assay was performed with the DNA relaxation kit supplied by Inspiralis Limited. In the assay performed, 0.5 µL (500 mg) of super-folded pBR322 DNA, 3 µL of assay buffer (Tris.HCl (10 $mmol \cdot L^{-1}$), NaCl (50 $mmol \cdot L^{-1}$), KCl (50 $mmol \cdot L^{-1}$), $MgCl_2$ (5.0 $mmol \cdot L^{-1}$), Na_2H_2EDTA (0.1 $mmol \cdot L^{-1}$), BSA (15 $mgmL^{-1}$) with pH 7.9), and 1µL of compound of interest at different concentrations, finally water and 1µL (4.0 $nmol \cdot L^{-1}$) of TOPOI were added to reach a final volume of 30 µL. The reaction mixture was kept in incubation at 37ºC for 40 minutes. After this period, 3 µL of SDS (sodium dodecyl sulfate) were added to the solution and a thermal shock was carried out at 60ºC for 2 min to interrupt the enzymatic process. After stopping the enzymatic action, 15 µL of STEB (40% (w/v) of sucrose, 100 $mmol \cdot L^{-1}$ of Tris.HCl, pH = 7.5, 1 $mmol \cdot L^{1}$ of EDTA, 0.5 $mgmL^{-1}$ of bromophenol blue) and 60µL of a mixture of chloroform:isoamyl alcohol (24:1 v/v). The samples were centrifuged at 5000 rpm

for 5 minutes, the aqueous phase was added to the 1% (w/v) agarose gel, in a 1x TBE buffer solution (Tris/Borate/EDTA) pH = 8.2. The same procedure was applied, showing in the interaction with super-coiled plasmid, the gel run and its development.

3.3.0 Inhibition of the DNA- topoisomerase II enzyme

The DNA-Topoisomerase IIα enzyme inhibition assay was performed with the DNA relaxation kit supplied by Inspiralis Limited. In the assay performed, 0.5 µL (500 mg) of super-folded pBR322 DNA, 3 µL of assay buffer (Tris.HCl (10 $mmol \cdot L^{-1}$), NaCl (50 $mmol \cdot L^{-1}$), KCl (50 $mmol \cdot L^{-1}$), $MgCl_2$ (5.0 $mmol \cdot L^{-1}$), Na_2H_2EDTA (0.1 $mmol \cdot L^{-1}$), BSA (15 $mgmL^{-1}$) with pH 7.9), 1µL (1, 0 $mmol \cdot L^{-1}$) of ATP and 1µL of compound of interest at different concentrations, finally water and 1µL (4.0 $nmol \cdot L^{-1}$) of TOPOII were added to reach a final volume of 30 µL. The reaction mixture was kept in incubation at 37ºC for 40 minutes. After this period, 3 µL of SDS (sodium dodecyl sulfate) were added to the solution and a thermal shock was carried out at 60ºC for 2 min to interrupt the enzymatic process. After stopping the enzymatic action, 15 µL of STEB (40% (w/v) of sucrose, 100 $mmol \cdot L^{-1}$ of Tris.HCl, pH = 7.5, 1 $mmol \cdot L^{-1}$ of EDTA, 0.5 $mgmL^{-1}$ of bromophenol blue) and 60µL of a mixture of chloroform:isoamyl alcohol (24:1 v/v). The samples were centrifuged at 5000 rpm for 5 minutes, the aqueous phase was added to the 1% (w/v) agarose gel, in a 1x TBE buffer solution (Tris/Borate/EDTA) pH = 8.2. The same procedure was applied, showing in the interaction with super-coiled plasmid, the gel run and its development.

3.3.1 Cathepsin B experimental protocol

To prepare the cathepsin B experiment, the cathepsin assay was done in each well for the three compounds in a 1200l mixture of Cathepsin B solution preparation (CTSB Reaction Buffer + CTSB Reagent + Cathepsin B) (compounds **1, 2,** and **3**). As a result, 10µl of enzyme control and 10µl of enzyme inhibitor (0.2µl CTSB inhibitior + 9.8µl CTSB Buffer) were added. Nonetheless, 10µl of each compound (Compound 1, 2, and 3) was added and incubated for 10-15

minutes at room temperature. Following incubation, 960µl of cathepsin B substrate (39.8µl CTSB Reaction Buffer +0.2µl CTSB substrate) was added to each well and fluorescence at Ex/Em 400/505nm in a kinetic mode of 30-60 minutes at 37^0C was measured.

Reagent preparation took place (by using the following kits components shown below). Hence, standard curve preparation follows.

TABLE 3.3 – Kits Components used for Cathepsin B preparation.

Item	Quantity
CTSB Reaction Buffer	15mL
CTSB Reagent	100µL
Cathepsin B	5µL
TSB Substrate, Ac-RR-AFC (10mM)	0.2mL
CTSB Inhibitor (F-F- FMK,1mM)	20µL

This further leads to the control and samples preparation. Moreover, the reaction is further observed and the measurement via the use of fluorescence at Ex/Em =400/500nm in a kinetic mode foe 30-60minutes at 37ºC was taken. Conclusively, calculation via data analysis took place. Importantly, when interpreting the result, it should be noted that cathepsin B substrate leads to fluorescence while cathepsin B substrate with Cathepsin B inhibitor leads to no fluorescence or decrease in fluorescence (FIGURE 3.5)

FIGURE 3.5**-** The difference between the results obtained when Cathepsin B lacks the inhibitor and Cathepsin B when the inhibitor is present.

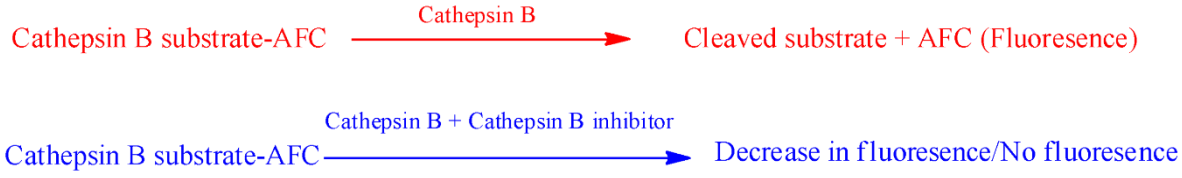

4.0 Results and discussion

The aim of this chapter is to discuss all synthetic results, techniques of characterisation, interaction with DNA, and the capacity to inhibit the action of cathepsin B.

Characterization

4.1 Nuclear Magnetic Resonance (NMR)

4.1.1 ^{1}H NMR

Attribute of the ^{1}H NMR signals was performed according to the numbering in the FIGURE 4.1 below. Also, this figure represents a general outline for the proposed structure of metal compounds **1-3**.

FIGURE 4.1- General Scheme of compounds with markings for the ^{1}HNMR spectra analysis.

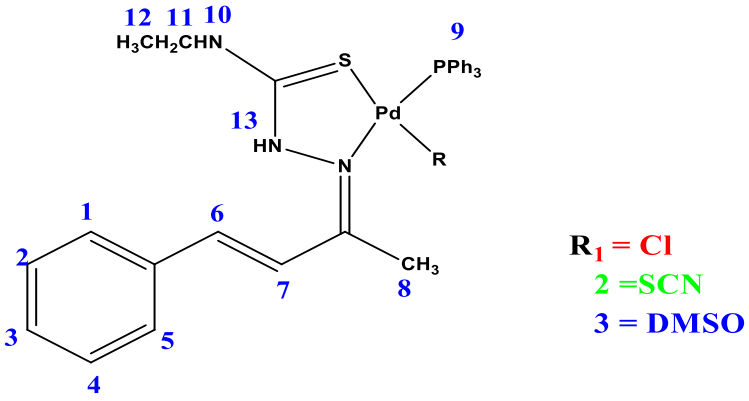

The following spectra shown below were obtained in deuterated chloroform ($CDCl_3$, d_1), which has a characteristic signal at 7.2 ppm [129]. The Spectra of each compounds are shown in the following FIGURE 4.2 to FIGURE 4.5. The chemical shifts and the number of calculated protons are presented in TABLE 4.1 with the due attributions.

TABLE 4.1- The chemical shifts of compounds **1**, **2**, and **3** in ^{1}H NMR are shown below, along with their ppm locations and peaks in brackets.

.

Compound 1	Compound 2	Compound 3	Atoms
0.0	0.0	0.0	**TMS**
1.22[3H]	1.14[3H]	1.14[3H]	**H_{12}**
3.22[2H]	3.29[2H]	3.30[2H]	**H_{11}**
2.64[3H]	2.39[4H]	2.46[3H]	**H_8**
7.20[1H]	7.12[1H]	7.01[1H]	**H_6**
8.48[1H]	8.15[1H]	8.57[1H]	**H_7**
7.67[2H]	7.66[2H]	7.68[2H]	**H_1 & H_5**
7.36[2H]	7.38[3H]	7.35[2H]	**H_2 & H_4**
7.26[4H]	7.26[3H]	7.26[3H]	**H_3**
7.76[5H], 7.50 [5H], 7.36[3H]	7.74[7H], 7.54[4H], 7.48[7H]	7.80[6H], 7.42[3H], 7.47[6H]	**H_9**

FIGURE 4.2- ^{1}H NMR spectrum in chloroform (d1) of the free ligand. The location of each structural bonds are carefully illustrated.

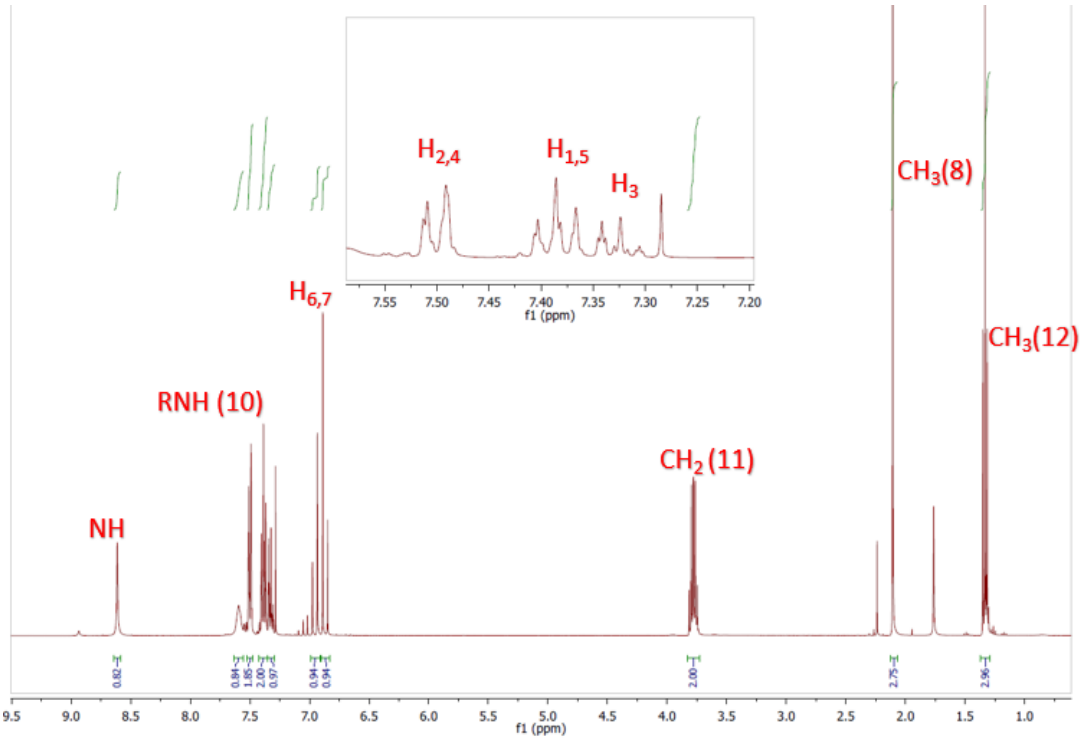

It was observed that the characteristic signals showed the free ligand with their respective integral's values. At downfield, the signals attributed to the

ethyl group were observed a triplet CH_3(12) at 1.33 ppm and a CH_2 multiple centered at 3.78 ppm. Also, the presence of a singlet was noted due to the methyl group CH_3 (8) at 2.11. Characteristic doublets, between 7.00-6.80 ppm, were observed for the trans olefinic hydrogens H6 and H7 with JHH of the 16.5 Hz. Aromatic hydrogens peaks occurred between 7.55-7.30 ppm. It was observed that the two doublets at 7.67 ppm refer to H1 and H5 once they are in the same chemical environment. At 7.36 ppm, signals related to H2 and H4 were also observed since they are symmetric to each other by a certain plane making them chemical equivalent. Finally, the thioamide hydrogen at 7.60 ppm and the acid iminic hydrogen at 8.81 were observed.

After coordinating the TSC ligand and co-ligands PPh_3, Cl^-, SCN^- and DMSO, it was possible to observe changes in the ^1H NMR signals attributed to TSC, the presence of peaks assigned to PPh_3 group and DMSO ligand (for complex **3**). Due to the similarity between them, the discussion was focused on complex **3**. It was possible to note displacement to up field on account of the withdrawal effects of the metal centers after complexation, mainly on the signals of CH3(8) close to the metal center and the TSC aromatic hydrogens. The peaks ascribed to the ethyl group were displacements to the downfield, probably due to the π back bonding involving the thioamide moiety. Also, the triphenylphosphine was noted between 7.36-7.76 ppm and the singlet attributed to DMSO hydrogen [6H] at 2.62ppm. Importantly, a coupling constant effect can be detected at atoms 6 and 7 in the spectrum, which is significant. It also means that the peak-to-peak distance, or J, is 16Hz.

FIGURE 4.3- ^1H NMR spectrum in chloroform (d1) of compound **1.** The below diagram depicts the precise location of hydrogen, as well as each ppm and its peak.

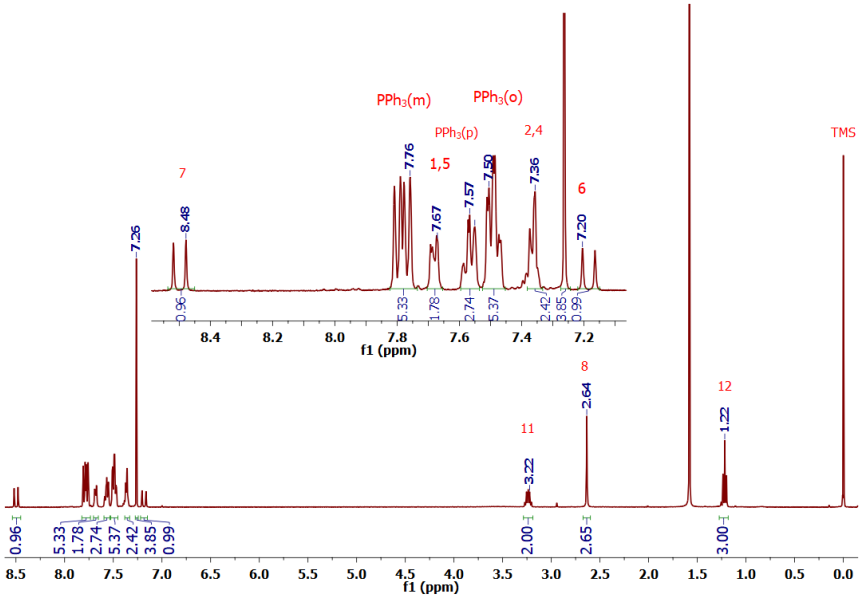

FIGURE 4.4- ^{1}H NMR spectrum in chloroform (d1) of compound **2.** The diagram below depicts the precise location of hydrogen, as well as each ppm and its peak.

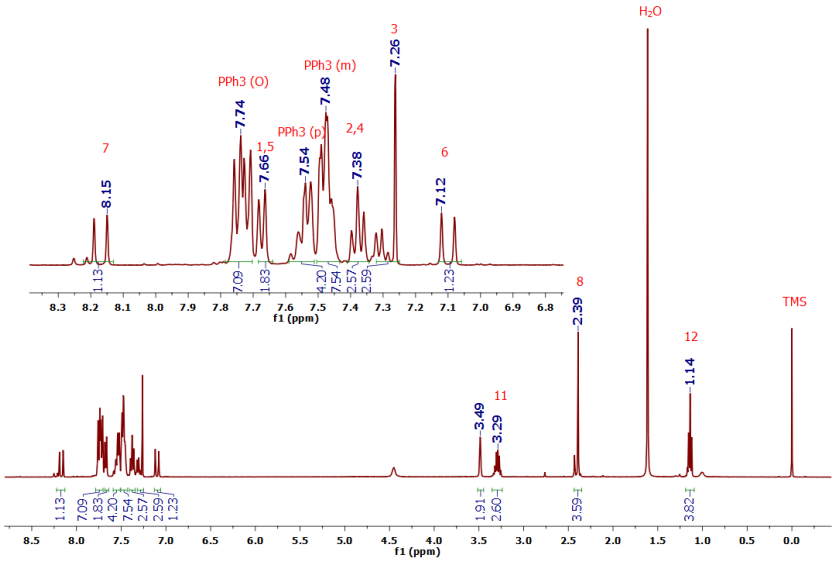

FIGURE 4.5- ^{1}H NMR spectrum in chloroform (d1) of compound **3.** The diagram below depicts the precise location of hydrogen, as well as each ppm and its peak.

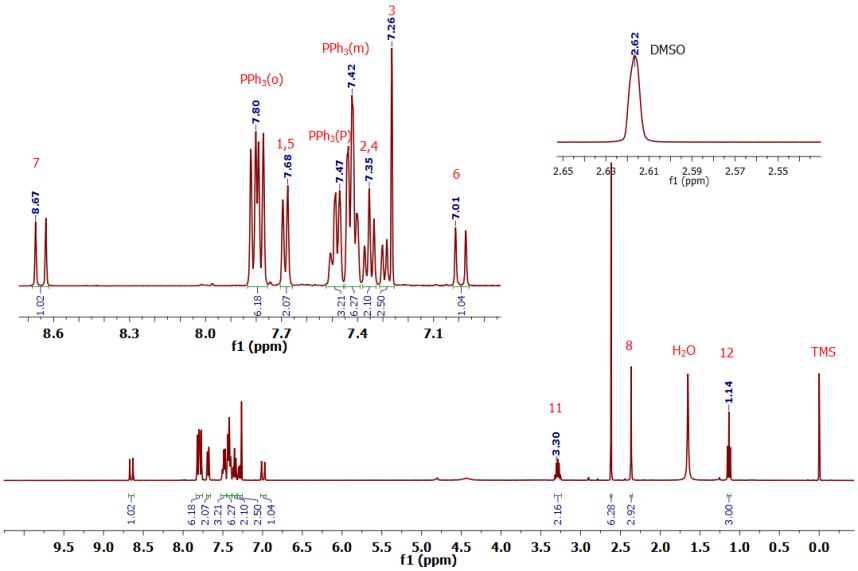

4.1.2 ^{31}P NMR

The ^{31}P NMR spectra were performed to observe if the coordination of the metal-bound phosphine group occurred. The ^{31}P NMR spectrum was taken just after the ^{1}H resonance, and the measurement was carried out with the same deuterated solution. The ^{31}P NMR spectra showed a shift of the phosphorus signal from the shielded region to the more unshielded part of the spectrum, this shift indicates the coordination of the phosphine to Pd(II), where the metal acts as an electron density stripper, thus decreasing the shielding of the core. The spectrum of triphenyl phosphine exemplifies the profile obtained for free phosphines (FIGURE 4.6) and the spectra obtained for compounds **1** to **3** are shown in FIGURE 4.7

FIGURE 4.6- ^{31}P NMR spectrum of triphenylphosphine [130]. The location of triphenylphosphine on the spectra below is shown when it is not attached to any other metals. When left alone, the location is always at the negative ppm.

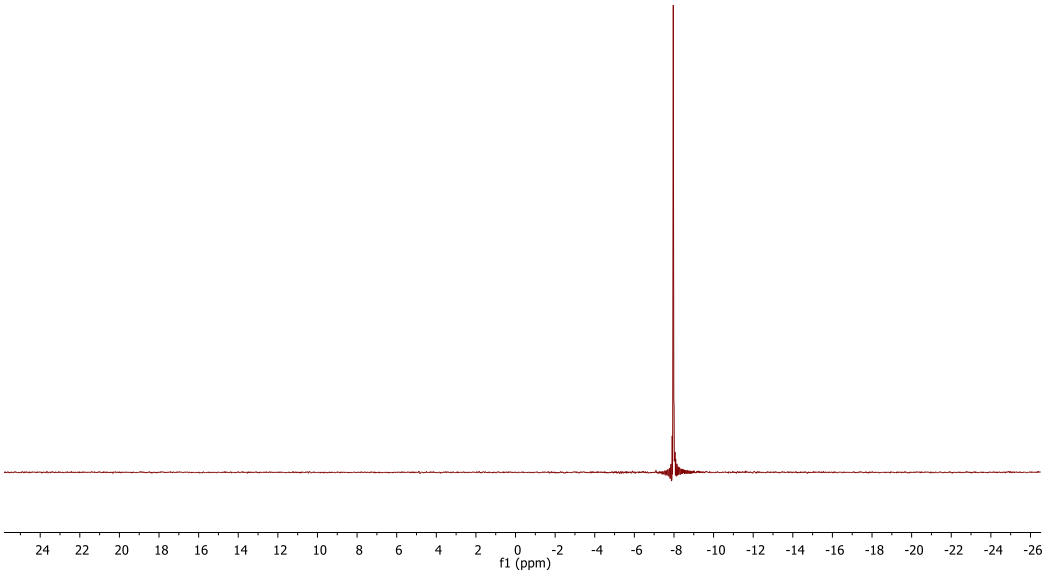

FIGURE 4.7- Shows ^{31}P NMR spectrum of compound **1,2** and **3** with triphenylphosphine respectively. Hence, the triphenylphosphine in the picture be is located at the positive side of the ppm because it is linked to the metal complex.

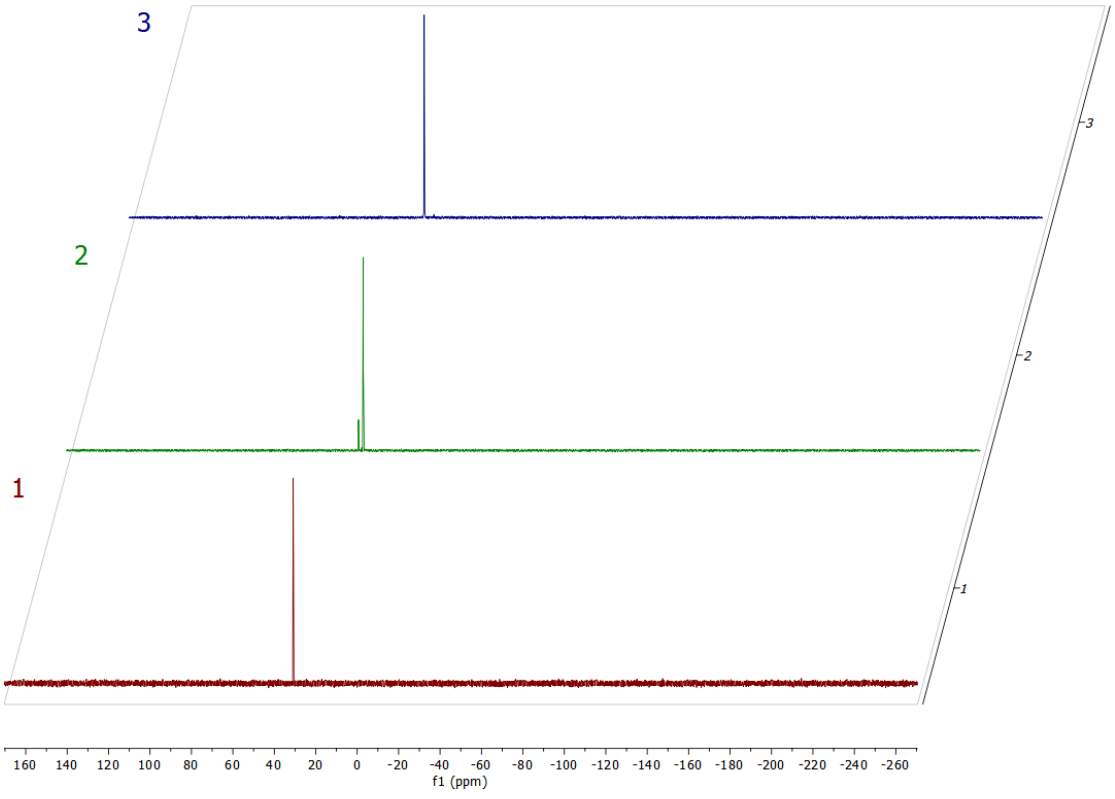

The observation shows that the coordination of the metal-bound phosphine group occurred. Literature [131] has proved that whenever phosphine group are alone, they are located at -7.3pm but for the spectrums above. The metal-bound phosphine groups are located between 20-40 ppm.

However much, it should be scrupulously observed that the spectrum for compound **2** is quite different from that of compound **1** and **3** since, the structure of compound **2** posses an ambidentate ligand which can perform two functions both in solid and liquid state. Hence, Compound **2** bond to a coordination center through nitrogen as well as sulphur (Pictorial Illustration shown in FIGURE 4.8 below).

FIGURE 4.8- shows the monodentate function of thiosemicarbazone. It further shows how sulphur binds to palladium also at another instance nitrogen perform the action of binding to palladium.

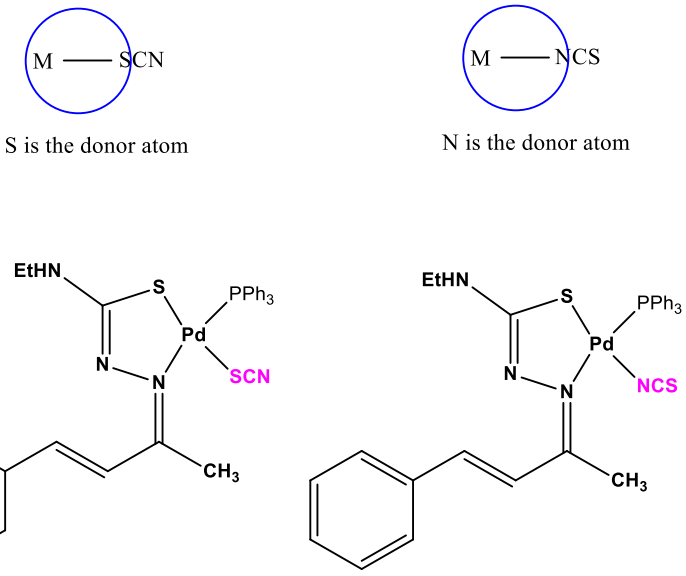

SCN can bond either through the sulphur atom or the nitrogen atom, but not at the same time.

4.2 Electronic spectroscopy in the UV-Visible region

The electronic spectra of the ligand and the complexes were performed in acetonitrile at a concentration of $1x10^{-5}$ mol·L^{-1}. FIGURE 4.9 shows the overlapping spectra. The spectrum of the ligand showed the highest values of

molar absorptivity (ε=13,237.62 $L \cdot mol^{-1} \cdot cm^{-1}$) among all compounds, presenting a band in a high energy region around 330 nm. Thus, the high absorptivity value found, together with its absorption region and bandwidth indicates an intra-ligand transition of type n→π*.

FIGURE 4.9- UV-Vis electronic spectra of complexes and ligand. The spectrum showed the wavelength of the ligand, start complex and palladium chloride complex separately. Hence, the palladium chloride complex showed no visible transition when observed while the ligand showed a transition around 290nm-390nm. This particularly region is further said to be specific to charge transfer. Lastly, the ligand showed and n- π* character. This further implies that the region is related to a charge transfer.

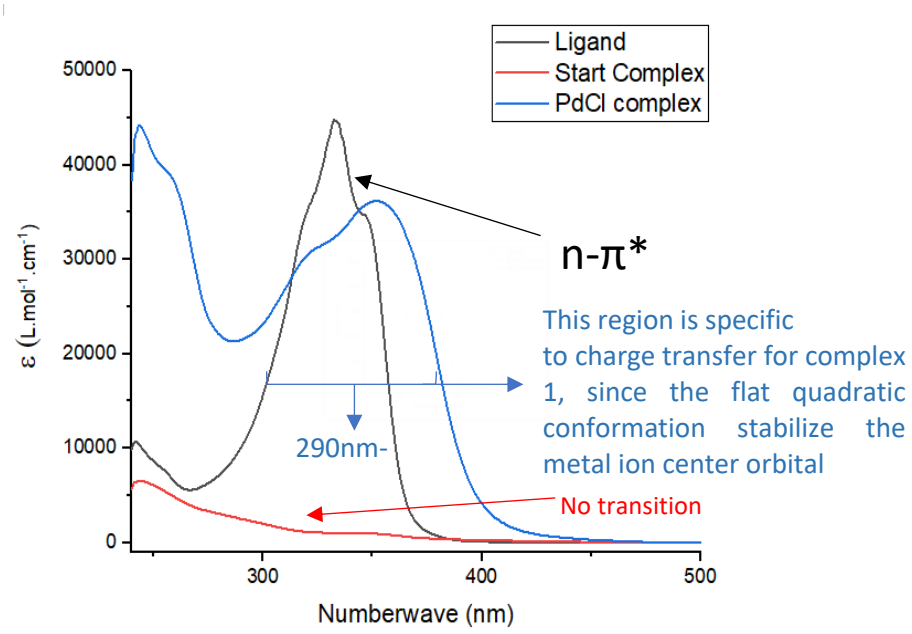

This type of intra-ligand transition commonly occurs in the ultraviolet region, because of its high energy in relation to charge transfers or MC band (metal centered), for example. Thus, the generation of an orbital node at the time of the electronic transition makes it very permissible, a fact that favors the interaction of electronic density with incident light according to TURRO et al [132].

The smaller number of atoms and consequently the smaller number of vibrational states makes the band narrower in relation to the complexes. The large number of σ bonds allows the molecule to still have accessible vibrational modes, which causes the band to widen in relation to more rigid ligands such as phenanthroline, which, for example, has a thin band at 290 nm [133].

It was observed that the complexes have wide bands in the region from 290 to 390 nm. And normally this region is related to Charge Transfer (MLCT or LMCT) for palladium complexes, since the flat quadratic conformation stabilizes the metal ion center orbitals, making them more energetically distant from the ligand orbitals, consequently, making the charge transition more energetic [134, 135].

FIGURE 4.10- UV-Vis electronic spectra of the overlapped compounds. In the picture above, all the compounds show a hypsochromic shift in relation to the spectrum of the free ligand above (Figure 4.9). This displacement is an indication that the coordination of the ligands to the metallic center has taken place.

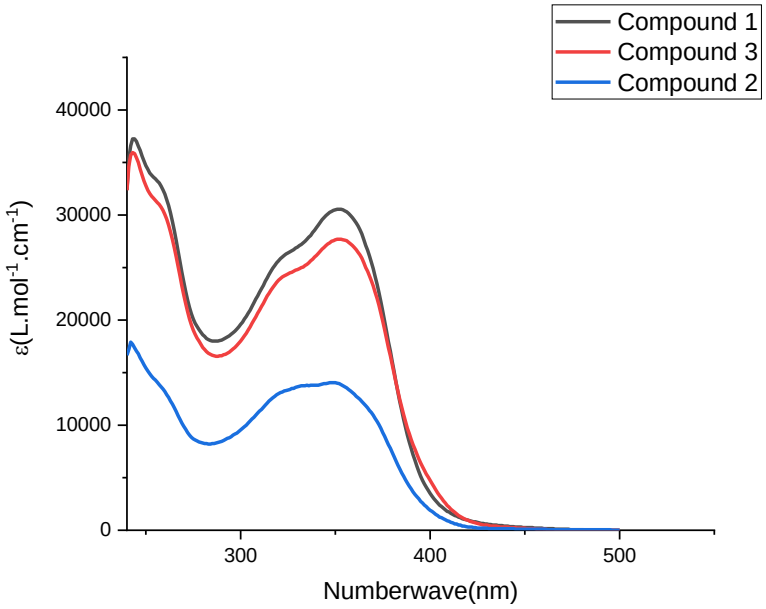

After the complexes has been reacted with the start compounds, all the three compounds showed a hypochromic shift in relation to the spectrum of the free ligands. It was observed that the compounds have wide bands in the region from 290 to 390 nm. Hence, this displacement is an indication that the coordination

of the ligands to the metallic center took place [134]. The hypochromic shift, also known as the blue shift, occurs when the band position in the spectrum shifts to a shorter wavelength. Observing that the flat quadratic conformation stabilizes the metal ion center orbitals, making them more energetically distant from the ligand orbitals, consequently, making the charge transition more energetic [125, 126]. Also, the acid π character of the associated ligands indicates an MLCT transition.

4.3 Vibrational Spectroscopy in Infrared Region

The spectra in the IR region of the compound **1-3** are shown in FIGURE 4.11 below, the main bands have been assigned and shown in TABLE 4.2.

FIGURE 4.11- IR spectra of the Pd(II) compounds and TSC obtained in KBr pallets.

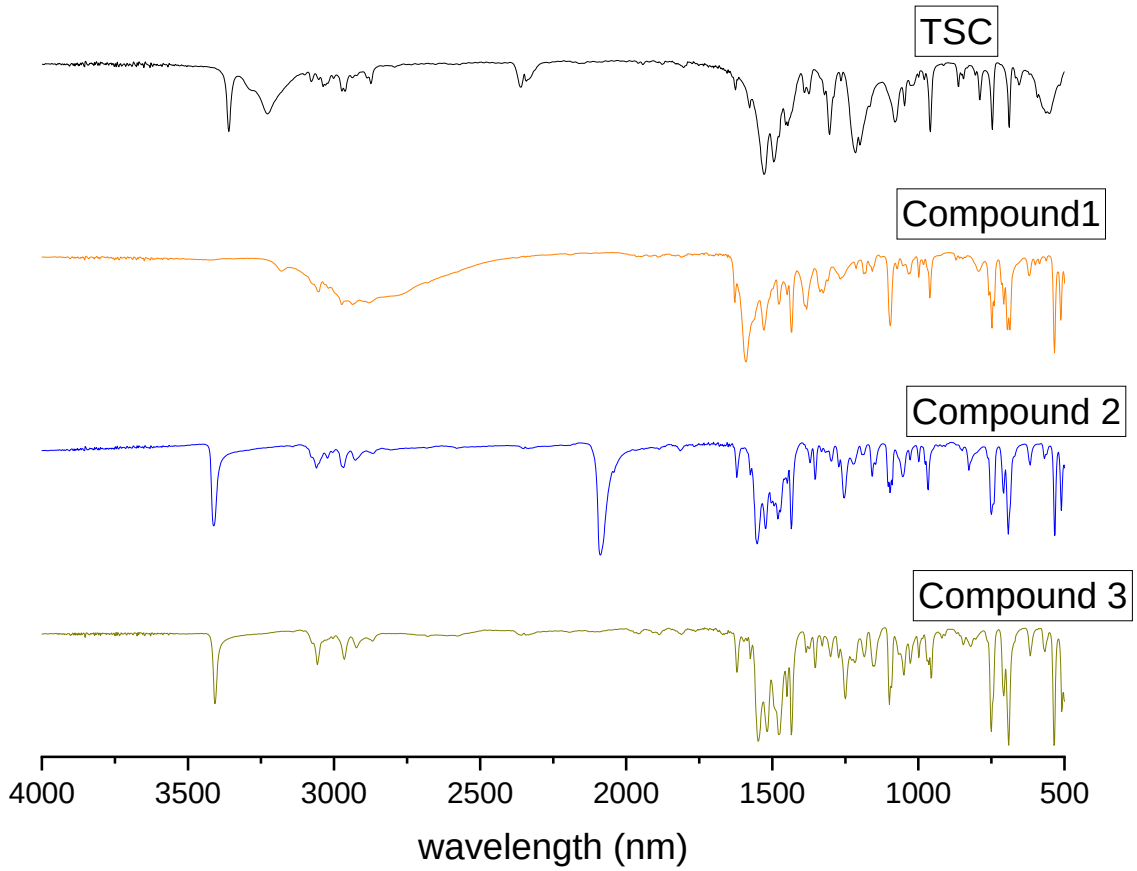

TABLE 4.2 - Main frequencies in the infrared region and attributions.

TSC	Compound 1	Compound 2	Compound 3	Attribution
3320	-	3410	3412	*ν* N-H(10)
3105	-	-	-	*ν* N-H(13)
2800	2800	2800	2800	*ν* C-H_3
1625	1625	1625	1625	*ν* C=N
–	1090	1090	1090	*ν* C-PPH3
–	–	–	800	*ν* DMSO
–	–	2125	-	*ν* SCN

In the free ligand spectrum, it is possible to highlight the diagnostic bands that can indicate coordination to the metal center. Initially, in high-energy regions, it is possible to observe the stretching of the NH(10) and NH(13) bonds occurring at 3320 cm^{-1} and 3105 cm^{-1}, respectively. At 2800 cm^{-1}, it is possible to notice the presence of bands referring to aliphatic CH stretches. A band is visible around 1625 cm^{-1}, which indicates the presence of a carbon-nitrogen bonding. The region between 1500-1350 cm^{-1} bands refers to C-C aromatic stretching. Comparing the spectra of the three compounds and the free ligand (TSC), one notices some modifications that indicate the coordination of the TSC, as well the other ligands. Initially, the band's presence at 1090 cm^{-1} is highlighted, referring to the stretching between the carbon and phosphorus atoms of triphenylphosphine, indicating the presence of the ligand in the molecular framework. Another critical finding occurs in the high-energy region, when it is possible to verify the absence of one of the NH bands due to the deprotonation of the TSC ligand and coordination to the metal, reinforcing this hypothesis, the displacement to energetic regions of stretching is noted. NH(10), characteristic of bidentate coordination of the ligand. Finally, compound 2 presents an intense band at 2125 cm-1 attributed to a sulfur

atom's thiocyanate ion coordination via terminal mode. This data shows that in solid-state, the system did not present the isomer isothiocyanate coordinated to the metal center as occurred in NRM spectra.

4.4 Mass Spectrometry

Mass spectrometry electron spray ionization (ESI-MS) is an important tool for determining the molecular mass of the ion/charge of the ion (m/z), and the isotopic pattern of organometallics and coordination compounds [136]. However, the use of this technique can cause high fragmentation, gain or loss of labile ligands, as well as oxidation and reduction of the analyzed compounds [127], and their capacity to keep their structure in solution. Figure 4.12 shows the mass spectrum for compound **1**. It was possible to observe the ion pic m/z at 650.076 with high accuracy (error of 1.54 ppm from the exact mass of the complex). However, due to the fragmentation process, the most intense pic was attributed to the compound without the chloride. Figure 4.12 presents the characteristic isotopic pattern for palladium.

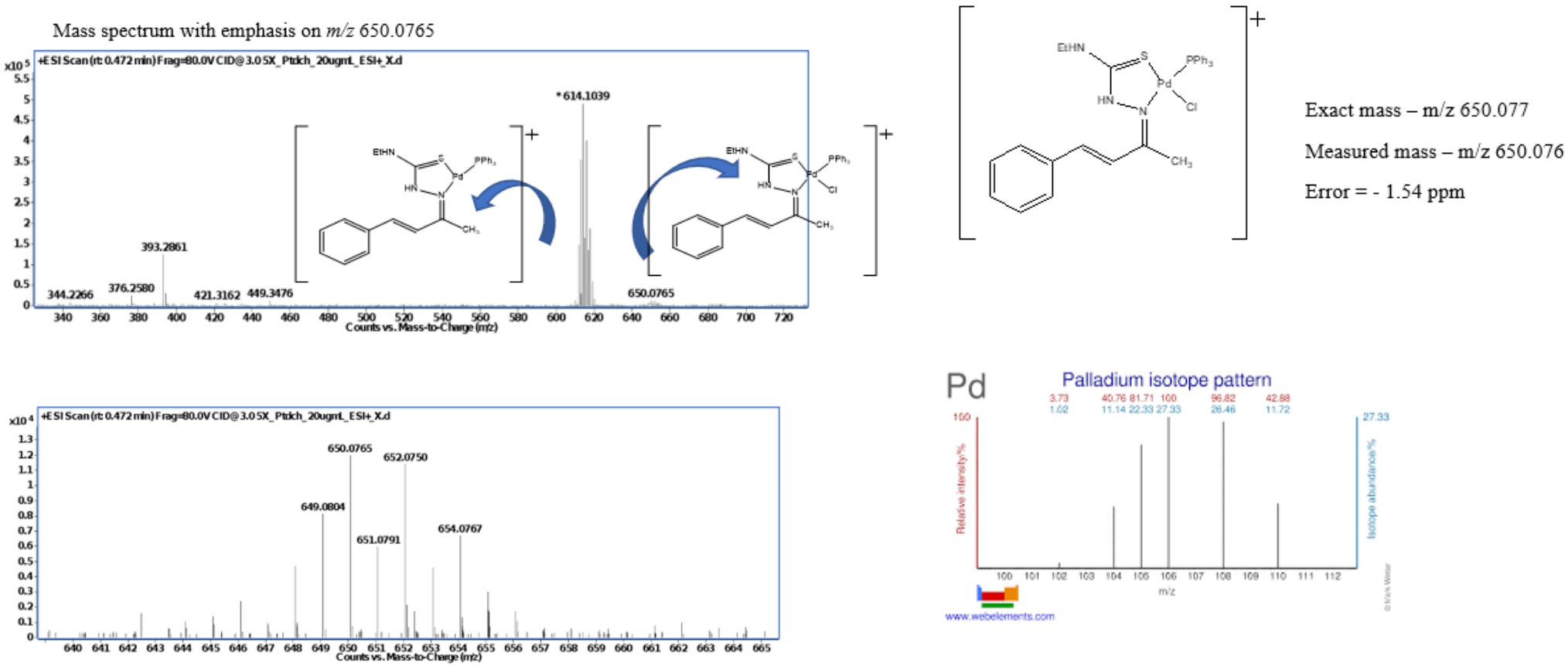

FIGURE 4.12 - General spectrum (a) and isotopic pattern (b) obtained by HRMS-ESI for the complex **1**. The mass spectrum on the top left highlighted the transition that occurred when chloride was introduced to the complex. As a result, the exact mass of the structure, as well as a negligible mistake in the ppm, can be seen on the right and side at the top. When looking at the left-hand side of the image at the bottom, it can be seen that the proposed complex **1** is within the needed ppm. Nonetheless, when compared to the work of jubribasic [137] , who experimented with Palladium Aminophosphonate Complexes on the right hand side. The differences were observed due to various neighbouring metal present.

4.5 Elemental Analysis

Elemental analysis is a process where a sample of material is analyzed for its elemental composition. Hence, quantitative elemental analysis was carried out to verify the proposal formular of each of the three compounds. More so, after the results, comparison took place to verify the credibility of each compound. Through the technique of elemental analysis, comparing the theoretical and experimental values, it was possible to see that both compound **1** and **3** quantities of carbon, hydrogen and nitrogen were in line with the gotten result. In addition, the purity was also confirmed. Nonetheless, Compound **2** nitrogen mass was different from the expected mass. Then new analysis will be performed to understand this situation.

TABLE 4.3- Elemental analysis for palladium (II) complexes

Complexes	C% exp (theory)	H% exp (theory)	N% exp (theory)
[Pd(TSC)ClPPh3] (1)	55.89 (57.15)	4.73 (4.95)	7.61 (6.45)
[Pd(TSC)SCNPPh$_3$] (2)	56.64 (57.01)	4.66 (4.78)	8.70 (8.31)
Pd-(TSC)-(CH$_3$)$_2$SOPPh$_3$] (3)	51.93 (51.80)	5.26 (5.01)	1.48 (5.49)

4.6 Single crystal X-ray diffraction

The crystals were obtained by crystallization in a solution saturated of the solubilized complexes a mixture of solvents of chloroform: acetonitrile (1:1). According to the protocol, it was possible to obtain crystals only for complex **1** sent to the Laboratory of Crystallography at the Institute of Chemistry of São Carlos (IQSC-USP) where he was X-ray diffraction performed.

The ORTEP representation with the atom labeling scheme is illustrated in FIGURE 4.13. The Pd(II) compounds adopts a distorted square-

planar geometry, with interatomic bond angles that deviated slightly from 90°. The bond lengths and the angles wherein the expected range (TABLE 4.4). TSC act as a neutral bidentate ligand, which led to a *cis* coordination through S1 and N1 atoms to form a five-membered ring. The remaining binding sites were occupied by a chloride ion that were coordinated *trans* to the S1 atom and with a phosphine ligand coordinated *trans* to the N1 atom. In the structure of compound **1**, it was possible to observe the presence of a chloride as a counter ion. The main X-ray diffraction data and parameters of the compound is showed in TABLE 4.5.

FIGURE 4.13-Structure of complex **1** obtained by X-ray diffraction analysis. The structure shows the locations of each atoms in relation to the central atom palladium.

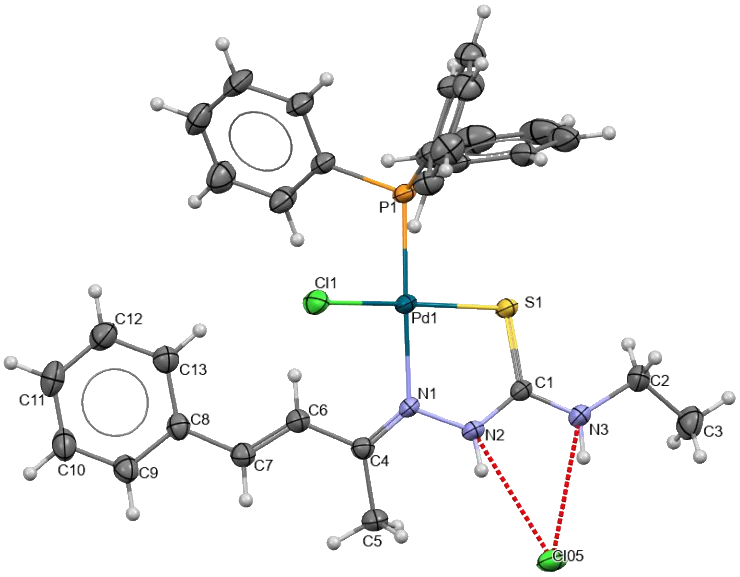

TABLE 4.4- Shows the interpretation of the above complex **1** X-ray diffraction diagram. It depicts the bond angles and bond lengths of the atoms in relation to the palladium complex.

Atoms	Angles^{o}	Atoms	Length/Å
S1-Pd1-Cl1	166.43(3)	**Pd1-Cl1**	2.3269(6)
P1-Pd1-Cl1	89.61(2)	**Pd1-S1**	2.2672(6)
P1-Pd1-S1	92.24(2)	**Pd1-P1**	2.2541(6)
N1-Pd1-Cl1	97.17(5)	**Pd1-N1**	2.1310(17)
N1-Pd1-S1	82.74(5)		
N1-Pd1-P1	170.47(6)		

TABLE 4.5- Shows the X-ray diffraction crystal data in addition with the parameters of the compounds.

X-ray diffraction data's	Values
Emperial formula	$C_{31}H_{32}Cl_2N_3PPdS$
Formula weight	686.92
Temperature/K	293(2)
Crystal system	Triclinic
Space group	P-1
a/Å	8.0497(3)
b/Å	12.0856(4)
c/Å	16.5953(5)
α/°	93.273(3)
β/°	98.749(3)
γ/°	101.680(3)
Volume/Å^3	1556.20(9)
Z	2
ρ_{calc}g/cm^3	1.466

μ/mm^{-1}	0.912
F(000)	700.0
Crystal size/mm^3	0.409 × 0.364 × 0.28
Radiation	Mo Kα (λ = 0.71073)
2Θ range for data collection/°	5.242 to 51.5
Index ranges	-9 ≤ h ≤ 9, -14 ≤ k ≤ 14, -20 ≤ l ≤ 20
Reflections collected	30876
Independent reflections	5947 [R_{int} = 0.0239, R_{sigma} = 0.0158]
Data/restraints/parameters	5947/0/354
Goodness-of-fit on F^2	1.167
Final R indexes [I>=2σ (I)]	R_1 = 0.0264, wR_2 = 0.0562
Final R indexes [all data]	R_1 = 0.0323, wR_2 = 0.0616
Largest diff. peak/hole / e $Å^{-3}$	0.52/-0.31

4.7 Cytotoxicity Assay

The determination of the cytotoxicity of the compounds was carried out using the colorimetric method MTT (3-(4,5-dimethylthiazol-2-yl)-2,5-diphenyl tetrazolium bromide). The assay was performed comparing cells treated with the compounds and untreated cells (control). The cells used for the assay were PNT2 (Non-Tumor Prostrate cell), A2780 Cis (Ovarian tumor cell lines) and MRC5 (non-tumor lung cell) to compare the preferences of the cytotoxic action of the complexes. Cisplatin was used as positive control.

The IC_{50} values obtained against the three cell lines are shown in table 4.6. From the analysis of these data is possible to note that: i) All the three complexes showed high cytotoxicity; ii) it should be noted that different cells determine if a greater or smaller concentration is the best when considering the cytotoxicity of each complex; iii) it is not observed a direct relation between the labile group and the cytotoxicity; iv) in general,

compounds showed a slight preference to A2780cis cells; v) Compound **3** surpass the action of cisplatin against A2780Cis in a 1400 fold; vi) All three compounds have shown to be very toxic to cancer cells and non-cancer cells because the values are shown are somewhat closer to each other. Thus, this kind of compound could be promising to obtain a prototype structure to generate high cytotoxicity agents. However, structural changes should be performed to modulate their selectivity.

TABLE 4.6- Cytotoxicity of Pd (II) compound **1**,**2** and **3** against strains of PNT2, A2780Cis and MRC-5.

Complexes	**PNT2**(μM)	**A2780Cis**(μM)	**MRC-5**(μM)
[Pd(TSC)ClPPh3] (1)	0.024±0.01	0.268±0.015	-
[Pd(TSC)SCNPPh$_3$] (2)	0.759±0.107	0.201±0.013	9.5±0.082
[Pd(TSC)(CH$_3$)$_2$SOPPh$_3$] (3)	1.582±0.107	0.017±0.004	5.346±0.002
Cisplatin	11.74±1.20	25.087±0.891	11.84±1.19

4.8 DNA Interaction

Spectroscopic titration

DNA interaction has been an essential component of the biological system. Hence, this experiment's target is to use spectroscopy in the UV-vis region to verify the absorptivity changes in the ct-DNA interaction. Thus, the interactions of transition metal compounds with DNA can be covalent or non-covalent. When a covalent interaction occurs, the labile ligand of the complexes is replaced by a nitrogenous DNA base, while non-covalent interactions include: intercalation, interaction with grooves, and electrostatic attraction. (FIGURE 4.14) shows the electronic spectra of the spectroscopic titration for compounds **1**, **2** and **3** at different concentrations. It further depicts the three compounds with DNA show no sign of interaction since neither significant change in the spectra was observed. Possibly, the

complex has a weak interaction that has been attributed to an electrostatic attraction, or an interaction in the DNA grooves, due to a hyperchromic effect. Once a covalent bond or intercalation leads to drastic alterations in the UV-vis spectrum profile.

FIGURE 4.14-Spectra in the UV-vis region of Pd (II) compound **1,2**,and **3** in the presence of different ct-DNA concentrations in DMSO.

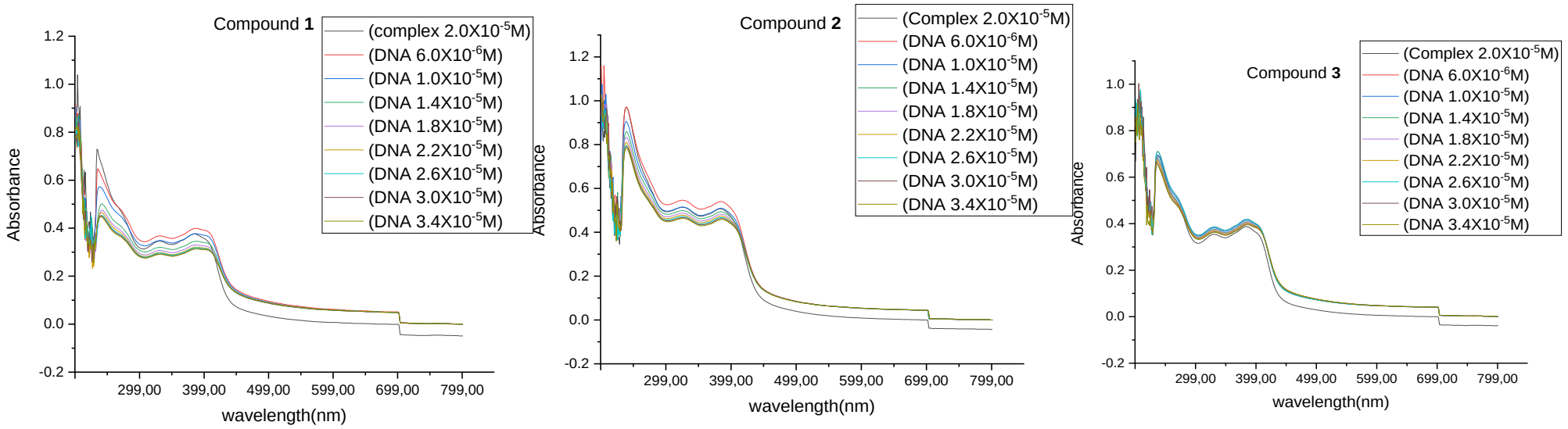

4.9 Inhibition of the DNA-Topoisomerase Iβ and IIα enzyme

Electrophoresis, a well-known and well-regarded technique, consisting in dragging molecules through a porous matrix (agarose gel). This dragging is performed by applying an electrical charge and a current on the gel, the DNA runs on the gel because of its negative charge at neutral or physiological pH (7.4). In this way, the plasmid runs in the gel from cathode to anode. There is a relationship between the mobility and size of the molecule. Super-coiled DNA has a smaller volume, being more compact than relaxed DNA. This conformational difference of the molecule affects its displacement through the gel. Thus, super-coiled DNA has greater mobility in the gel than relaxed DNA. Due to this particularity, it is possible to observe changes in the shape of the DNA through retention in the electrophoresis gel [138].

FIGURE 4.15-Schematic representation of plasmid DNA forms observed by agarose gel electrophoresis [138].

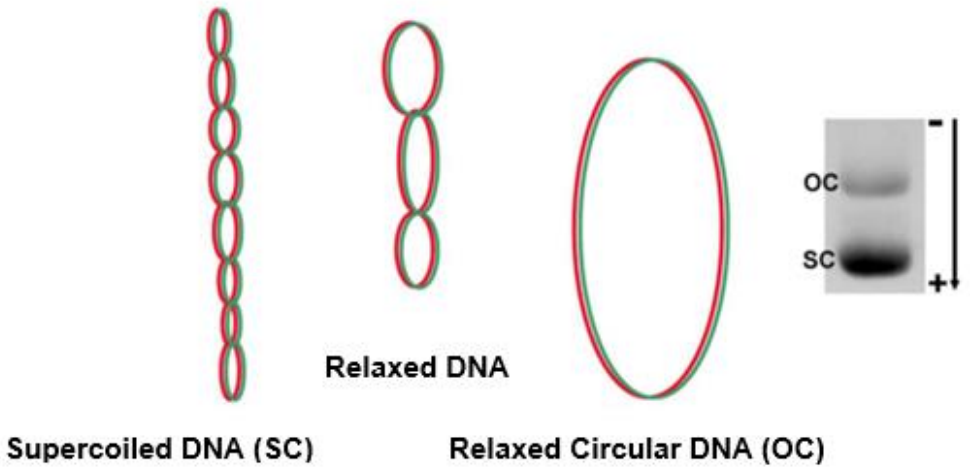

Topoisomerases are nuclear enzymes that plays essential roles in DNA transcription, replication chromosome segregation, and recombination. They are important targes of approved and experimental anti-

cancer agents. All cells have two major forms of topoisomerases: type I enzymes (which makes single strands cut in DNA) and type II enzyme (which cut and pass double strand DNA). Nonetheless, as it is known that topoisomerases are important for DNA duplication, and it is related to overexpression in cancer cells. The importance of this topoisomerase assay is to assess new compounds entities for their ability to inhibit both forms of topoisomerase.

The DNA-Topoisomerase I & II inhibition assay was performed with the kit provided by Inspiralis Limited, using plasmid pBR322 (supercoiled DNA), which was incubated with all complexes individually at two different concentrations, 5 and 12.5 $\mu mol \cdot L^{\neg -1}$. The result obtained showed the best inhibition of the enzyme associated with compounds **1, 2**, and **3** (FIGURE 4.16 & 4.17). In this assay below (Topoisomerase Iβ), it was showed that in the lane **3** to lane **11**, there was partial inhibition of the enzyme that is, the presence of super-tangled DNA. Which further implies that the three compounds showed a possible interaction with the enzyme.

FIGURE 4.16- Inhibitory capacity of TOPO Iβ enzyme by compound **1** to **3**. Lane 1: plasmid ($3\ \mu mol \cdot L^{-1}$ Buffer, $0.5\ \mu mol \cdot L^{-1}$ plasmid DNA topoisomerase, and $26.5\ \mu mol \cdot L^{-1}$ water). Lane 2: ($3\ \mu mol \cdot L^{-1}$ Buffer, $0.5\ \mu mol \cdot L^{-1}$ DNA, $1\ \mu mol \cdot L^{-1}$ water, and $26.5\ \mu mol \cdot L^{-1}$ water). Lane 3: ($1\ \mu mol \cdot L^{-1}$). Lane 4: ($10\ \mu mol \cdot L^{-1}$). Lane 5: ($100\ \mu mol \cdot L^{-1}$). Lane 6: ($1\ \mu mol \cdot L^{-1}$). Lane 7: ($10\ \mu mol \cdot L^{-1}$). Lane 8: ($100\ \mu mol \cdot L^{-1}$). Lane 9: ($1\ \mu mol \cdot L^{-1}$). Lane 10: ($10\ \mu mol \cdot L^{-1}$). Lane 11: ($100\ \mu mol \cdot L^{-1}$).

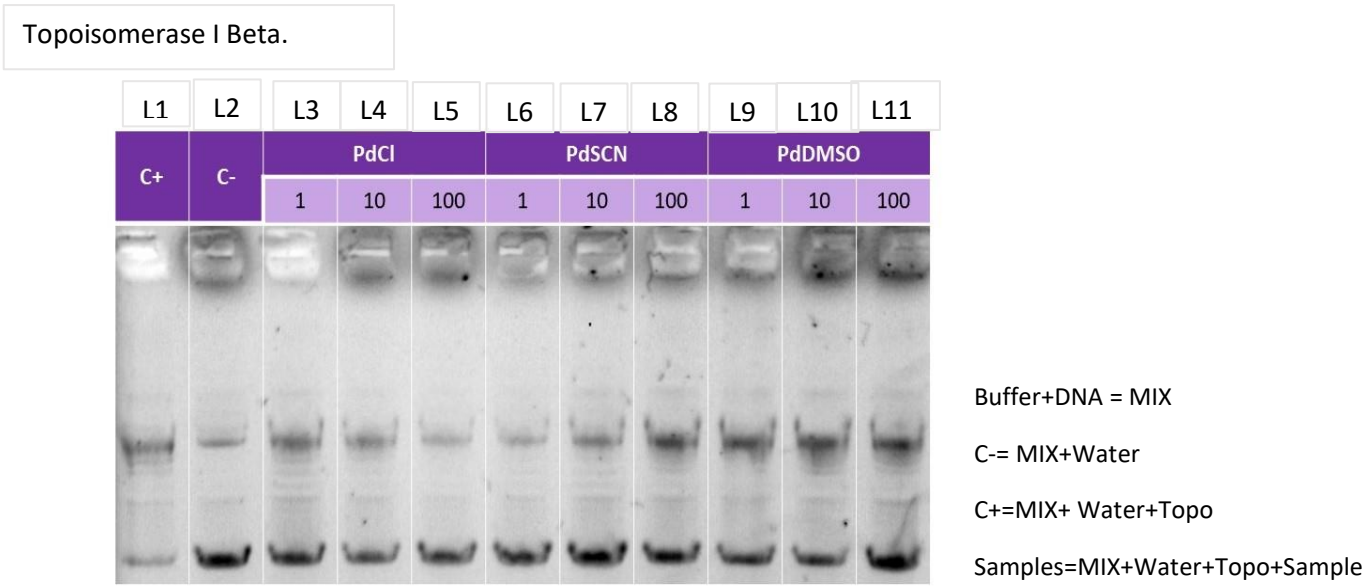

FIGURE 4.17- Inhibitory capacity of topoisomerase IIα enzyme by compound **1** to **3**. Lane 1: plasmid (3 μmol·L^{-1} Buffer, 0.5 μmol·L^{-1} plasmid DNA topoisomerase,1 μmol·L^{-1} ATP and 25.5 μmol·L^{-1} water). Lane 2: (3 μmol·L^{-1} Buffer, 0.5 μmol·L^{-1} DNA, 1 μmol·L^{-1} water, and 26.5 μmol·L^{-1} water). Lane 3: (1 μmol·L^{-1}). Lane 4: (10 μmol·L^{-1}). Lane 5: (100 μmol·L^{-1}). Lane 6: (1 μmol·L^{-1}). Lane 7: (10 μmol·L^{-1}). Lane 8: (100 μmol·L^{-1}). Lane 9: (1 μmol·L^{-1}). Lane 10: (10 μmol·L^{-1}). Lane 11: (100 μmol·L^{-1}).

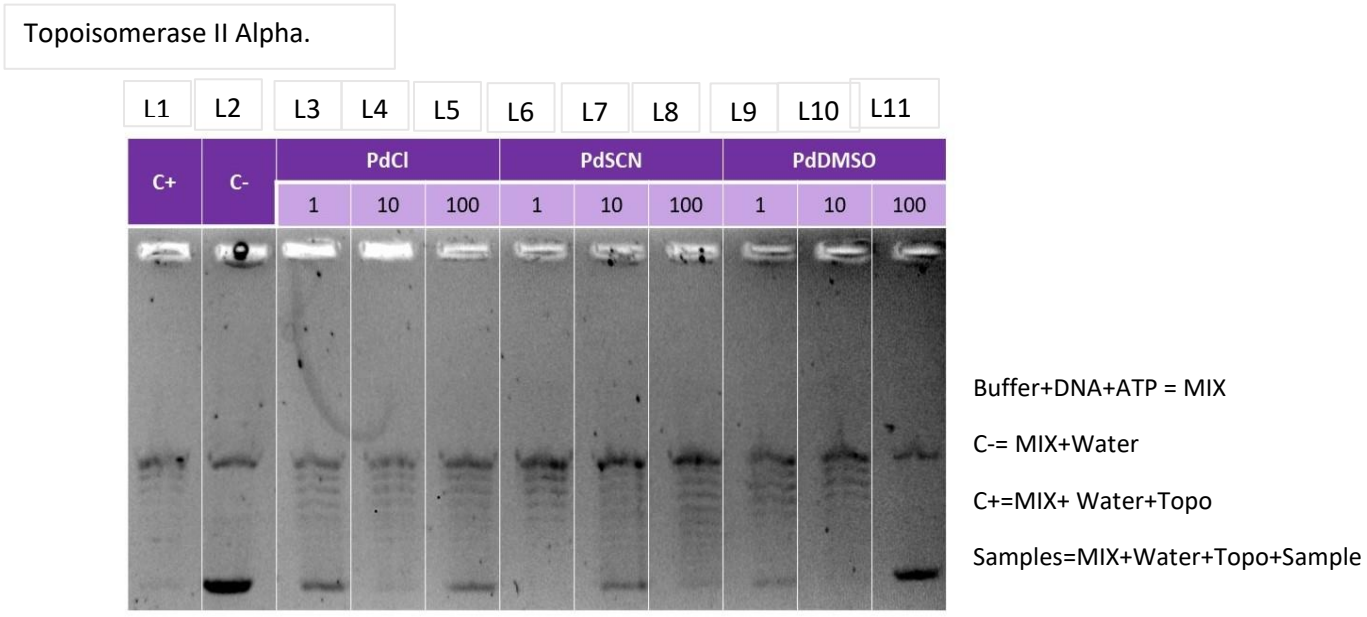

In this assay above (Topoisomerase IIα), it was observed that in the lane 3 to lane 11, there was no inhibition of the enzyme. Hence, there are no indications that the complexes stop the relaxation of DNA provide by the topoisomerase IIα enzyme.

4.10 Inhibition of Cathepsin B

Cathepsin B (CTSB, EC 3.4.22.1) is a lysosomal cysteine proteinase that is suggested to participate in intracellular degradation and turnover of proteins. It has also been implicated in tumor invasion and metastasis. Hence, Abcam's Cathepsin B Inhibitor Screening Kit (ab185438) was purchased. Abcam's Cathepsin B Inhibitor Screening Kit utilizes the ability of Cathepsin B to cleave the synthetic AFC based peptide substrate to

release AFC, which can be easily quantified using a fluorometer or fluorescence microplate reader. In the presence of a Cathepsin B-specific inhibitor, the cleavage of the substrate is reduced/abolished resulting in decrease or total loss of the AFC fluorescence. This high-throughput adaptable assay kit is simple, sensitive, and rapid tool to screen the potential inhibitors of Cathepsin B. Set of investigation was carried out on the potential inhibitory effect of Palladium (II) compounds (**1-3**) against cathepsin B. The three Palladium II compounds (compounds **1-3**) were assayed against Cathepsin B at seven different concentrations (from 300µL to 25 µL) following the above assay procedures. Hence, the data analysis obtained from fluorescence was further calculated via the slope for all test Inhibitor Samples [S] and Enzyme Control (EC) by dividing the net ΔRFU (RFU2-RFU1) values with the time ΔT (T2-T1).

The relative activity of the three compounds were shown versus their concentrations. Furthermore, with IC_{50} values ranging from 60.27 to 100.7 µM, these drugs inhibited cysteine proteases (TABLE 4.7). The results showed that the inhibition capacity of the compounds changes depending on the labile group. Compound **2** with SCN^- as ligand showed the lowest value of IC_{50}, probably due to their strong interaction with the palladium ion. Although chloride is a greater leaving group than DMSO, it is possible to note an inversion of the IC_{50} values. It can be related to stereo hindrance to entrance into the activity pocket of the enzyme. Nevertheless, more studies must be executed to confirm this hypothesis. FIGURE 4.18 shows the inhibition capacity of the complexes at 100 µM through time. It is possible to observe that all the three compounds act in the same way of the irreversible pattern (positive control). Also, DMSO compound has a close ratio of inhibition of positive control. These results indicate that palladium compounds are a good strategy to afford inhibitors of cathepsin B. However, mores comprehension of the system is necessary to propose a prototype compound that has a great capacity to inhibit the enzyme target with an adequate labile group and structural volume to achieve the activity pocket.

TABLE 4.7- Compounds with their IC_{50} values

Compounds	IC_{50} (μM)
$Pd(TSC)ClPPh_3$ **(1)**	86.37
$Pd(TSC)SCNPPh_3$ **(2)**	100.7
$Pd(TSC)(DMSO)PPh_3$ **(3)**	60.27

FIGURE 4.18- Comparison of the inhibition capacity among Compounds **1**, **2** and **3** with both enzyme control (C-) and Enzyme Inhibitor (C+). The diagram elaborated how the compounds act in the same threshold of irreversible pattern but at different RFU. Even though the inhibition capacity of the three compounds differs from each other, they all fall in between the enzyme control and enzyme inhibitor. This further explained how the novel compounds plays an inhibitory role to Cathepsin B.

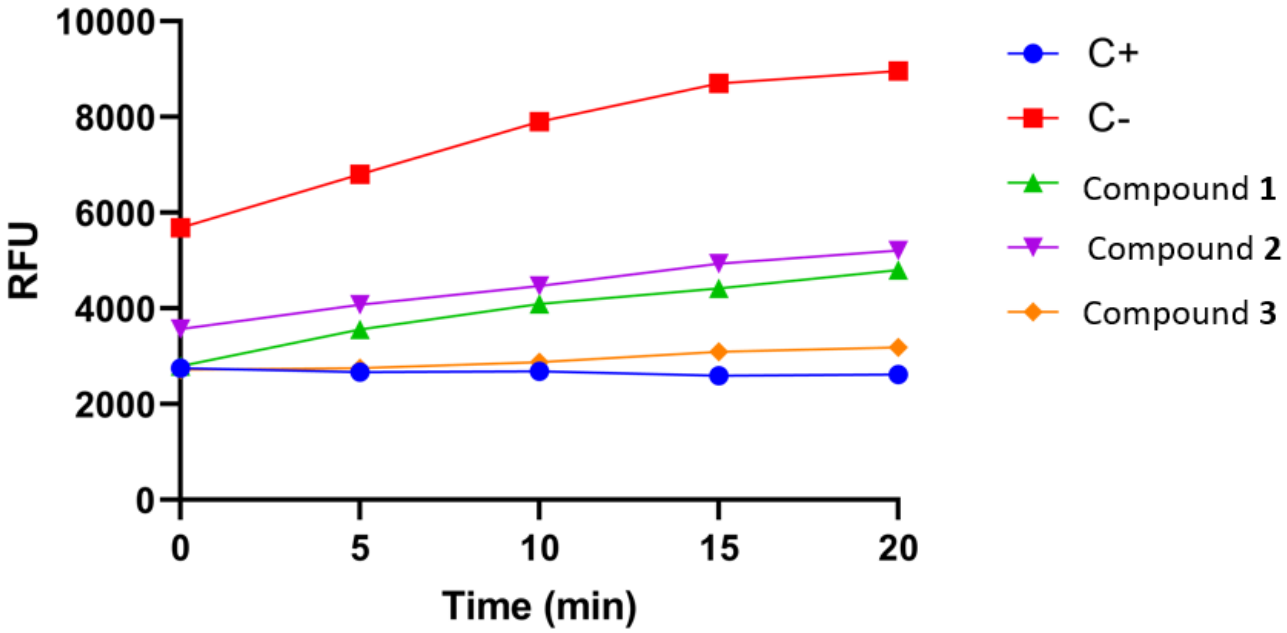

5.0 Conclusion

In this work, three new palladium (II) compounds were characterized by UV-vis, NMR, infrared elemental analysis and mass spectrometry. In which it was possible to demonstrate coordination. After the characterizations of the coordination compounds, they were DNA interaction studies were performed using spectroscopy in the UV-vis. The results indicated that all the three compounds do not exhibit any form of significant interactions. Which further implies that the complex has a weak interaction that has been attributed to an electrostatic attraction, or an interaction in the DNA grooves, due to a hyperchromic effect.

However, the next test which was cytotoxicity was carried out on the three compounds. The cytotoxicity assays for the assessment of cytotoxicity against following cell lines are PNT2 (Non-Tumor Prostrate cell), A2780 Cis (Ovarian tumor cell lines) and MRC-5 (non-tumor lung cell). The result obtained revealed high inhibitory activity of the compounds. All the three compounds showed greater cytotoxicity.

Progressively, When the inhibitory actions of the three compounds were tested on topoisomerase II alpha, there was no evidence that the compounds acted on it, although there was partial inhibition on topoisomerase I beta. The assessment of the inhibitory capacity of complexes against cathepsin B enzyme provided important information about a possible medium of action. The three compounds performed an irreversible inhibition. Compound **3** has a substantially larger inhibitory effect with a low RFU value. Conclusively, this research showed that the structural features proposed can generate high cytotoxicity compounds that’s inhibit the action of cathepsin B. Nevertheless, the compounds do not present any selectivity towards tumor cells and non-tumor cells. Further, a greater understanding of the activity mode against cathepsin B will help to propose new improvements on the molecular framework.

References.

1. Salvesen, G.S.J.T.J.o.c.i., *A lysosomal protease enters the death scene.* 2001. **107**(1): p. 21-23.
2. Frlan, R. and S. Gobec, *Inhibitors of cathepsin B.* Curr Med Chem, 2006. **13**(19): p. 2309-27.
3. Lichtenstein, N. and J.S.J.P.o.t.N.A.o.S.o.t.U.S.o.A. Fruton, *Studies on beef spleen cathepsin A.* 1960. **46**(6): p. 787.
4. Greenbaum, L.M. and J.S.J.J.o.B.C. Fruton, *Purification and properties of beef spleen cathepsin B.* 1957. **226**(1): p. 173-180.
5. Tallan, H.H., M.E. Jones, and J.S.J.J.o.B.C. Fruton, *On the Proteolytic Enzymes of Animal Tissues: X. Beef Spleen Cathepsin C.* 1952. **194**(2): p. 793-805.
6. Press, E., R. Porter, and J.J.B.J. Cebra, *The isolation and properties of a proteolytic enzyme, cathepsin D, from bovine spleen.* 1960. **74**(3): p. 501.
7. Lapresle, C. and T.J.B.J. Webb, *The purification and properties of a proteolytic enzyme, rabbit cathepsin E, and further studies on rabbit cathepsin D.* 1962. **84**(3): p. 455.
8. Dingle, J.T., et al., *Proteoglycan-degrading enzymes. A radiochemical assay method and the detection of a new enzyme cathepsin F.* 1977. **167**(3): p. 775-785.
9. Malemud, C.J. and A.J.A.o.t.N.Y.A.o.S. Janoff, *Human polymorphonuclear leukocyte elastase and cathepsin G mediate the degradation of lapine articular cartilage proteoglycan.* 1975. **256**: p. 254-262.
10. Kirschke, H.J.A.b.e.m.G., *Cathepsin H: an endoaminopeptidase.* 1977. **36**(11-12): p. 1547-1548.
11. Liao, J.C., J.F.J.B. Lenney, and b.r. communications, *Cathepsins J and K: high molecular weight cysteine proteinases from human tissues.* 1984. **124**(3): p. 909-916.
12. Kirschke, H., et al., *Cathepsin L: A New Proteinase from Rat-Liver Lysosomes.* 1977. **74**(2): p. 293-301.
13. Velasco, G., et al., *Human cathepsin O. Molecular cloning from a breast carcinoma, production of the active enzyme in Escherichia coli, and expression analysis in human tissues.* 1994. **269**(43): p. 27136-27142.
14. Kirschke, H., I. Schmidt, and B.J.B.J. Wiederanders, *Cathepsin S The cysteine proteinase from bovine lymphoid tissue is distinct from cathepsin L (EC 3.4. 22.15).* 1986. **240**(2): p. 455-459.
15. Hargrove, J.L., et al., *Cathepsin T (convertase) generates the multiple forms of tyrosine aminotransferase by limited proteolysis.* 1982. **21**(2): p. 283-289.
16. Adachi, W., et al., *Isolation and characterization of human cathepsin V: a major proteinase in corneal epithelium.* 1998. **39**(10): p. 1789-1796.
17. Linnevers, C., S. Smeekens, and D.J.F.l. Brömme, *Human cathepsin W, a putative cysteine protease predominantly expressed in CD8+ T-lymphocytes.* 1997. **405**(3): p. 253-259.
18. Sakamoto, E., et al., *Cathepsin Y (a novel thiol enzyme) produces kinin potentiating peptide from the component protein of rat plasma.* 1999. **45**(1-3): p. 207-214.
19. Santamaría, I., et al., *Cathepsin Z, a novel human cysteine proteinase with a short propeptide domain and a unique chromosomal location.* 1998. **273**(27): p. 16816-16823.
20. Turk, V., J. Kos, and B.J.C.c. Turk, *Cysteine cathepsins (proteases)—on the main stage of cancer?* 2004. **5**(5): p. 409-410.
21. Brix, K., et al., *Cysteine cathepsins: cellular roadmap to different functions.* 2008. **90**(2): p. 194-207.
22. Tardy, C., et al., *Lysosomes and lysosomal proteins in cancer cell death (new players of an old struggle).* 2006. **1765**(2): p. 101-125.

23. Zavašnik-Bergant, T. and B. Turk, *Cysteine proteases: destruction ability versus immunomodulation capacity in immune cells.* 2007.
24. Gocheva, V. and J.A.J.C.c. Joyce, *Cysteine cathepsins and the cutting edge of cancer invasion.* 2007. **6**(1): p. 60-64.
25. Vasiljeva, O., et al., *Emerging roles of cysteine cathepsins in disease and their potential as drug targets.* 2007. **13**(4): p. 387-403.
26. Sigloch, F.C., et al., *Proteomic analysis of silenced cathepsin B expression suggests non-proteolytic cathepsin B functionality.* 2016. **1863**(11): p. 2700-2709.
27. Formolo, C.A., et al., *Secretome signature of invasive glioblastoma multiforme.* 2011. **10**(7): p. 3149-3159.
28. Fong, D., et al., *Confirmation of the human cathepsin B gene (CTSB) assignment to chromosome 8.* 1992. **89**(1): p. 10-12.
29. Lin, L., et al., *A minimal critical region of the 8p22–23 amplicon in esophageal adenocarcinomas defined using sequence tagged site-amplification mapping and quantitative polymerase chain reaction includes the GATA-4 gene.* 2000. **60**(5): p. 1341-1347.
30. Fonović, M. and B.J.B.e.B.A.-g.s. Turk, *Cysteine cathepsins and extracellular matrix degradation.* 2014. **1840**(8): p. 2560-2570.
31. Gondi, C.S. and J.S.J.E.o.o.t.t. Rao, *Cathepsin B as a cancer target.* 2013. **17**(3): p. 281-291.
32. Murnane, M.J., et al., *Stage-specific increases in cathepsin B messenger RNA content in human colorectal carcinoma.* 1991. **51**(4): p. 1137-1142.
33. Krepela, E., J. Vicar, and M.J.N. Cernoch, *Cathepsin B in human breast tumor tissue and cancer cells.* 1989. **36**(1): p. 41-52.
34. Uchiyama, Y.J.A.o.h. and cytology, *Autophagic cell death and its execution by lysosomal cathepsins.* 2001. **64**(3): p. 233-246.
35. Wu, D., et al., *Cathepsin B may be a potential biomarker in cervical cancer.* 2012.
36. Kuang, F., et al., *Cathepsin B is a mediator of organelle-specific initiation of ferroptosis.* 2020. **533**(4): p. 1464-1469.
37. Rawlings, N.D., et al., *MEROPS: the database of proteolytic enzymes, their substrates and inhibitors.* 2014. **42**(D1): p. D503-D509.
38. Musil, D., et al., *The refined 2.15 A X-ray crystal structure of human liver cathepsin B: the structural basis for its specificity.* Embo j, 1991. **10**(9): p. 2321-30.
39. Turk, B., D. Turk, and V. Turk, *Lysosomal cysteine proteases: more than scavengers.* Biochim Biophys Acta, 2000. **1477**(1-2): p. 98-111.
40. Illy, C., et al., *Role of the occluding loop in cathepsin B activity.* J Biol Chem, 1997. **272**(2): p. 1197-202.
41. Cygler, M., et al., *Structure of rat procathepsin B: model for inhibition of cysteine protease activity by the proregion.* Structure, 1996. **4**(4): p. 405-16.
42. Sloane, B.F., et al., *Cathepsin B and its endogenous inhibitors: the role in tumor malignancy.* Cancer Metastasis Rev, 1990. **9**(4): p. 333-52.
43. Akinyemi, A.O., G.B.S. Pereira, and F.V.J.M.R.i.M.C. Rocha, *Role of cathepsin B in cancer progression: a potential target for coordination compounds.* 2021.
44. McCormick, D., *Secretion of cathepsin B by human gliomas in vitro.* Neuropathol Appl Neurobiol, 1993. **19**(2): p. 146-51.
45. Rozhin, J., et al., *Pericellular pH affects distribution and secretion of cathepsin B in malignant cells.* Cancer Res, 1994. **54**(24): p. 6517-25.
46. Maciewicz, R.A., et al., *Susceptibility of the cartilage collagens types II, IX and XI to degradation by the cysteine proteinases, cathepsins B and L.* FEBS Lett, 1990. **269**(1): p. 189-93.

47. Mort, J.S. and D.J. Buttle, *Cathepsin B.* Int J Biochem Cell Biol, 1997. **29**(5): p. 715-20.
48. Man, S.M. and T.D. Kanneganti, *Regulation of lysosomal dynamics and autophagy by CTSB/cathepsin B.* Autophagy, 2016. **12**(12): p. 2504-2505.
49. Podgorski, I. and B.F. Sloane, *Cathepsin B and its role(s) in cancer progression.* Biochem Soc Symp, 2003(70): p. 263-76.
50. Blass, G., et al., *Chronic cathepsin inhibition by E-64 in Dahl salt-sensitive rats.* Physiol Rep, 2016. **4**(17).
51. Riccio, M., et al., *Nuclear localization of cystatin B, the cathepsin inhibitor implicated in myoclonus epilepsy (EPM1).* Exp Cell Res, 2001. **262**(2): p. 84-94.
52. Cheng, X.W., et al., *Role for cysteine protease cathepsins in heart disease: focus on biology and mechanisms with clinical implication.* Circulation, 2012. **125**(12): p. 1551-62.
53. Padamsey, Z., et al., *Activity-Dependent Exocytosis of Lysosomes Regulates the Structural Plasticity of Dendritic Spines.* Neuron, 2017. **93**(1): p. 132-146.
54. Wassélius, J., et al., *Cathepsin B in the rat eye.* Graefes Arch Clin Exp Ophthalmol, 2003. **241**(11): p. 934-42.
55. Bengsch, F., et al., *Cell type-dependent pathogenic functions of overexpressed human cathepsin B in murine breast cancer progression.* 2014. **33**(36): p. 4474-4484.
56. Sloane, B.F., et al., *Membrane association of cathepsin B can be induced by transfection of human breast epithelial cells with c-Ha-ras oncogene.* 1994. **107**(2): p. 373-384.
57. Ma, W., et al., *Detection of esophageal squamous cell carcinoma by cathepsin B activity in nude mice.* 2014. **9**(3): p. e92351.
58. Bao, W., et al., *Silencing of Cathepsin B suppresses the proliferation and invasion of endometrial cancer.* 2013. **30**(2): p. 723-730.
59. Berquin, I.M., et al., *Identification of two new exons and multiple transcription start points in the 5'-untranslated region of the human cathepsin-B-encoding gene.* 1995. **159**(2): p. 143-149.
60. Yan, Z., et al., *Oncogenic c-Ki-ras but not oncogenic c-Ha-ras up-regulates CEA expression and disrupts basolateral polarity in colon epithelial cells.* 1997. **272**(44): p. 27902-27907.
61. Health, M.o., *Cancer Fundamentals, Secretary of Medical Assistance* National Cancer Division; Brasilia, 1971: p. 7-47.b.
62. Health, M.o., *National Cancer Institute Accessed* Brasil.
63. Organisation., W.H. and *Key Statistics.* **Accessed December 9, 2019**.
64. Silva, J.A.G.o., *Brasil, Ministry of Health,.* National Cancer Institute, Accessed December 9, 2019.
65. Gondi, C.S. and J.S. Rao, *Cathepsin B as a cancer target.* Expert Opin Ther Targets, 2013. **17**(3): p. 281-91.
66. Krepela, E., J. Vicar, and M. Cernoch, *Cathepsin B in human breast tumor tissue and cancer cells.* Neoplasma, 1989. **36**(1): p. 41-52.
67. Kos, J., et al., *Cysteine proteinases and their inhibitors in extracellular fluids: markers for diagnosis and prognosis in cancer.* Int J Biol Markers, 2000. **15**(1): p. 84-9.
68. Krepela, E., et al., *Increased cathepsin B activity in human lung tumors.* Neoplasma, 1990. **37**(1): p. 61-70.
69. Rempel, S.A., et al., *Cathepsin B expression and localization in glioma progression and invasion.* Cancer Res, 1994. **54**(23): p. 6027-31.
70. Sinha, A.A., et al., *Cathepsin B expression is similar in African-American and Caucasian prostate cancer patients.* Anticancer Res, 2007. **27**(5a): p. 3135-41.
71. Fernández, P.L., et al., *Expression of cathepsins B and S in the progression of prostate carcinoma.* Int J Cancer, 2001. **95**(1): p. 51-5.

72. Kostoulas, G., et al., *Stimulation of angiogenesis through cathepsin B inactivation of the tissue inhibitors of matrix metalloproteinases.* FEBS Lett, 1999. **455**(3): p. 286-90.
73. Kos, J., A. Mitrović, and B. Mirković, *The current stage of cathepsin B inhibitors as potential anticancer agents.* Future Med Chem, 2014. **6**(11): p. 1355-71.
74. Alabi, Z.O., et al., *The Role of BFl-1 in Cancer Unravels Inhibition Mechanism.*
75. Buck, M.R., et al., *Degradation of extracellular-matrix proteins by human cathepsin B from normal and tumour tissues.* Biochem J, 1992. **282 (Pt 1)**(Pt 1): p. 273-8.
76. Ishidoh, K. and E. Kominami, *Procathepsin L degrades extracellular matrix proteins in the presence of glycosaminoglycans in vitro.* Biochem Biophys Res Commun, 1995. **217**(2): p. 624-31.
77. Guinec, N., et al., *"In vitro" digestion of intact bovine lens capsules by four human lysosomal cysteine-proteinases.* Biol Chem Hoppe Seyler, 1990. **371 Suppl**: p. 239-54.
78. Guinec, N., V. Dalet-Fumeron, and M. Pagano, *"In vitro" study of basement membrane degradation by the cysteine proteinases, cathepsins B, B-like and L. Digestion of collagen IV, laminin, fibronectin, and release of gelatinase activities from basement membrane fibronectin.* Biol Chem Hoppe Seyler, 1993. **374**(12): p. 1135-46.
79. Yan, S., M. Sameni, and B.F. Sloane, *Cathepsin B and human tumor progression.* Biol Chem, 1998. **379**(2): p. 113-23.
80. Frosch, B.A., et al., *Molecular regulation, membrane association and secretion of tumor cathepsin B.* Apmis, 1999. **107**(1): p. 28-37.
81. Koblinski, J.E., M. Ahram, and B.F. Sloane, *Unraveling the role of proteases in cancer.* Clin Chim Acta, 2000. **291**(2): p. 113-35.
82. Wu, D., et al., *Cathepsin B may be a potential biomarker in cervical cancer.* Histol Histopathol, 2012. **27**(1): p. 79-87.
83. Satelur, K.P., et al., *Role of Cathepsin B as a Marker of Malignant Transformation in Oral Lichen Planus: An Immunohistochemical Study.* J Clin Diagn Res, 2017. **11**(8): p. Zc29-zc32.
84. Pandey, G., et al., *Prognostic and therapeutic relevance of cathepsin B in pediatric acute myeloid leukemia.* Am J Cancer Res, 2019. **9**(12): p. 2634-2649.
85. Herszényi, L., et al., *[Role and behavior of cathepsin B and cathepsin L in gastric cancer].* Orv Hetil, 1995. **136**(25): p. 1315-8.
86. Nishikawa, H., et al., *The role of cathepsin B and cystatin C in the mechanisms of invasion by ovarian cancer.* Gynecol Oncol, 2004. **92**(3): p. 881-6.
87. Chan, A.T., et al., *Cathepsin B expression and survival in colon cancer: implications for molecular detection of neoplasia.* Cancer Epidemiol Biomarkers Prev, 2010. **19**(11): p. 2777-85.
88. Nouh, M.A., et al., *Cathepsin B: a potential prognostic marker for inflammatory breast cancer.* J Transl Med, 2011. **9**: p. 1.
89. Gupta, R., et al., *uPAR/cathepsin B overexpression reverse angiogenesis by rescuing FAK phosphorylation in uPAR/cathepsin B down regulated meningioma.* PLoS One, 2011. **6**(2): p. e17123.
90. Yanamandra, N., et al., *Blockade of cathepsin B expression in human glioblastoma cells is associated with suppression of angiogenesis.* Oncogene, 2004. **23**(12): p. 2224-30.
91. Ruan, J., et al., *Over-expression of cathepsin B in hepatocellular carcinomas predicts poor prognosis of HCC patients.* Mol Cancer, 2016. **15**: p. 17.
92. Bian, B., et al., *Cathepsin B promotes colorectal tumorigenesis, cell invasion, and metastasis.* Mol Carcinog, 2016. **55**(5): p. 671-87.
93. Cheriyath, V., et al., *Potentiation of apoptosis by histone deacetylase inhibitors and doxorubicin combination: cytoplasmic cathepsin B as a mediator of apoptosis in multiple myeloma.* Br J Cancer, 2011. **104**(6): p. 957-67.

94. Kusunoki, T., et al., *Study on cathepsin B activity in human thyroid tumors.* Auris Nasus Larynx, 1995. **22**(1): p. 43-8.
95. Liang, S., et al., *Inhibition of cathepsin B activity prevents deterioration in the quality of in vitro aged porcine oocytes.* Theriogenology, 2018. **116**: p. 103-111.
96. Pelosi, G.J.T.O.C.J., *Thiosemicarbazone metal complexes: from structure to activity.* 2010. **3**(1).
97. Finch, R.A., et al., *Triapine (3-aminopyridine-2-carboxaldehyde thiosemicarbazone; 3-AP): an inhibitor of ribonucleotide reductase with antineoplastic activity.* 1999. **39**: p. 3-12.
98. French, F.A. and E.J.J.C.r. Blanz, *The carcinostatic activity of α-(N) heterocyclic carboxaldehyde thiosemicarbazones: I. Isoquinoline-1-carboxaldehyde thiosemicarbazone.* 1965. **25**(9 Part 1): p. 1454-1458.
99. Raghav, N. and R.J.M.C.R. Kaur, *Synthesis and evaluation of some semicarbazone-and thiosemicarbazone-based cathepsin B inhibitors.* 2014. **23**(11): p. 4669-4679.
100. Lima, M.A., et al., *Palladium (II) complexes bearing thiosemicarbazone and phosphines as inhibitors of DNA-Topoisomerase II enzyme: Synthesis, characterizations and biological studies.* 2020. **112**: p. 107708.
101. Brockman, R., et al., *Heterocyclic thiosemicarbazones: correlation between structure, inhibition of ribonucleotide reductase, and inhibition of DNA viruses.* 1970. **133**(2): p. 609-614.
102. Shao, J., et al., *A Ferrous-Triapine complex mediates formation of reactive oxygen species that inactivate human ribonucleotide reductase.* 2006. **5**(3): p. 586-592.
103. Yuan, J., D.B. Lovejoy, and D.R.J.B. Richardson, *Novel di-2-pyridyl–derived iron chelators with marked and selective antitumor activity: in vitro and in vivo assessment.* 2004. **104**(5): p. 1450-1458.
104. Wu, C.-P., et al., *Evidence for dual mode of action of a thiosemicarbazone, NSC73306: a potent substrate of the multidrug resistance–linked ABCG2 transporter.* 2007. **6**(12): p. 3287-3296.
105. Wangpu, X., et al., *Targeting the metastasis suppressor, N-Myc downstream regulated gene-1, with novel di-2-pyridylketone thiosemicarbazones: Suppression of tumor cell migration and cell-collagen adhesion by inhibiting focal adhesion kinase/paxillin signaling.* 2016. **89**(5): p. 521-540.
106. Pahontu, E., et al., *Antibacterial, antifungal and in vitro antileukaemia activity of metal complexes with thiosemicarbazones.* 2015. **19**(4): p. 865-878.
107. Ruiz, J., et al., *Novel bis-C,N-cyclometalated iridium(III) thiosemicarbazide antitumor complexes: interactions with human serum albumin and DNA, and inhibition of cathepsin B.* Inorg Chem, 2013. **52**(2): p. 974-82.
108. Rosenberg, B., et al., *Platinum compounds: a new class of potent antitumour agents.* 1969. **222**(5191): p. 385-386.
109. Knoll, J.D. and C.J.C.c.r. Turro, *Control and utilization of ruthenium and rhodium metal complex excited states for photoactivated cancer therapy.* 2015. **282**: p. 110-126.
110. Fung, S.K., et al., *Cyclometalated Gold (III) Complexes Containing N-Heterocyclic Carbene Ligands Engage Multiple Anti-Cancer Molecular Targets.* 2017. **129**(14): p. 3950-3954.
111. Tsuji, J.J.A.o.C.R., *Carbon-carbon bond formation via palladium complexes.* 1969. **2**(5): p. 144-152.
112. Kapdi, A.R. and I.J.J.C.S.R. Fairlamb, *Anti-cancer palladium complexes: a focus on PdX 2 L 2, palladacycles and related complexes.* 2014. **43**(13): p. 4751-4777.
113. Motswainyana, W.M., et al., *Imino-phosphine palladium (II) and platinum (II) complexes: Synthesis, molecular structures and evaluation as antitumor agents.* 2013. **129**: p. 112-118.

114. Lease, N., et al., *Potential anticancer heterometallic Fe–Au and Fe–Pd agents: initial mechanistic insights.* 2013. **56**(14): p. 5806-5818.
115. Matović, Z.D., et al., *Antitumor effects of a tetradentate amido-carboxylate ligands and corresponding square-planar palladium (II) complexes toward some cancer cells. Crystal structure, DFT modeling and ligand to DNA probe Docking simulation.* 2013. **121**: p. 134-144.
116. Bincoletto, C., et al., *Chiral cyclopalladated complexes derived from N, N-dimethyl-1-phenethylamine with bridging bis (diphenylphosphine) ferrocene ligand as inhibitors of the cathepsin B activity and as antitumoral agents.* 2005. **13**(8): p. 3047-3055.
117. Askari, B., et al., *Synthesis, solution behaviour and potential anticancer activity of new trinuclear organometallic palladium (II) complex of {S}-1-phenylethyl dithiooxamide: Comparison with the trinuclear heterobimetallic platinum (II) analogue.* 2019. **164**: p. 195-201.
118. Fricker, S.P., et al., *Metal compounds for the treatment of parasitic diseases.* J Inorg Biochem, 2008. **102**(10): p. 1839-45.
119. Carretero, J.C. and R.G.J.E.o.R.f.O.S. Arrayás, *Dichloro Bis (acetonitrile) Palladium.* 2001.
120. Treu-Filho, O., et al., *Molecular structures and vibrational frequencies for [PdX2 (tdmPz)](X= Cl−, SCN−): A DFT study.* 2009. **921**(1-3): p. 239-243.
121. Faraglia, G. and S.J.I.c.a. Sitran, *The behaviour of dithiocarbamic ester palladium (II) and platinum (II) complexes in dimethyl sulfoxide.* 1990. **176**(1): p. 67-73.
122. Dolomanov, O.V., et al., *OLEX2: a complete structure solution, refinement and analysis program.* 2009. **42**(2): p. 339-341.
123. Sheldrick, G.M.J.A.C.S.A.F. and Advances, *SHELXT–Integrated space-group and crystal-structure determination.* 2015. **71**(1): p. 3-8.
124. Bourhis, L.J., et al., *The anatomy of a comprehensive constrained, restrained refinement program for the modern computing environment–Olex2 dissected.* 2015. **71**(1): p. 59-75.
125. Barra, C.V., et al., *DNA binding, topoisomerase inhibition and cytotoxicity of palladium (II) complexes with 1, 10-phenanthroline and thioureas.* 2016. **446**: p. 54-60.
126. Popolin, C.P., et al., *Cytotoxicity and anti-tumor effects of new ruthenium complexes on triple negative breast cancer cells.* 2017. **12**(9): p. e0183275.
127. Colina-Vegas, L., et al., *Ru (II)/clotrimazole/diphenylphosphine/bipyridine complexes: Interaction with DNA, BSA and biological potential against tumor cell lines and Mycobacterium tuberculosis.* 2016. **162**: p. 135-145.
128. Reichmann, M., et al., *A further examination of the molecular weight and size of desoxypentose nucleic acid.* 1954. **76**(11): p. 3047-3053.
129. Gottlieb, H.E., V. Kotlyar, and A.J.J.o.O.C. Nudelman, *NMR chemical shifts of common laboratory solvents as trace impurities.* 1997. **62**(21): p. 7512-7515.
130. Dunne, B. and A.J.A.C.S.C.C.S.C. Orpen, *Triphenylphosphine: a redetermination.* 1991. **47**(2): p. 345-347.
131. Bhattacharya, S., et al., *Bioinspired oxidation of oximes to nitric oxide with dioxygen by a nonheme iron (II) complex.* 2020. **25**(1): p. 3-11.
132. Turro, N.J., et al., *Principles of molecular photochemistry: an introduction*. 2009: University science books.
133. Sastri, C., et al., *DNA interactions of new mixed-ligand complexes of cobalt (III) and nickel (II) that incorporate modified phenanthroline ligands.* 2003. **94**(1-2): p. 138-145.
134. Bandyopadhyay, N., et al., *Synthesis, structure, DFT calculations, electrochemistry, fluorescence, DNA binding and molecular docking aspects of a novel oxime based ligand and its palladium (II) complex.* 2016. **160**: p. 336-346.

135. Pattanayak, P., et al., *Synthesis and characterization of palladium (II) complex of Schiff base ligand: CS bond cleavage and catalytic activity.* 2015. **53**: p. 68-71.
136. McIndoe, J.S. and K.L.J.J.o.M.S. Vikse, *Assigning the ESI mass spectra of organometallic and coordination compounds.* 2019. **54**(5): p. 466-479.
137. Juribašić, M., et al., *Electrospray ionization mass spectrometry of palladium(II) quinolinylaminophosphonate complexes.* J Am Soc Mass Spectrom, 2011. **22**(10): p. 1815-25.
138. Barra, C.V. and A.V.J.R.V.d.Q. Netto, *Interações entre Complexos Antitumorais e o DNA e suas Ferramentas de Análise: um Enfoque nos Metalointercaladores.* 2015. **7**(6): p. 1998-2016.